nature geoscience

ARTICLES

https://doi.org/10.1038/s41561-019-0430-7

Sponge skeletons as an important sink of silicon in the global oceans

Manuel Maldonado[1]*, María López-Acosta[1], Cèlia Sitjà[1], Marta García-Puig[1], Cristina Galobart[1], Gemma Ercilla[2] and Aude Leynaert[3]

Silicon (Si) is a pivotal element in the biogeochemical and ecological functioning of the ocean. The marine Si cycle is thought to be in internal equilibrium, but the recent discovery of Si entries through groundwater and glacial melting have increased the known Si inputs relative to the outputs in the global oceans. Known outputs are due to the burying of diatom skeletons or their conversion into authigenic clay by reverse weathering. Here we show that non-phototrophic organisms, such as sponges and radiolarians, also facilitate significant Si burial through their siliceous skeletons. Microscopic examination and digestion of sediments revealed that most burial occurs through sponge skeletons, which, being unusually resistant to dissolution, had passed unnoticed in the biogeochemical inventories of sediments. The preservation of sponge spicules in sediments was 45.2 ± 27.4%, but only 6.8 ± 10.1% for radiolarian testa and 8% for diatom frustules. Sponges lead to a global burial flux of 1.71 ± 1.61 TmolSi yr^{-1} and only 0.09 ± 0.05 TmolSi yr^{-1} occurs through radiolarians. Collectively, these two non-phototrophically produced silicas increase the Si output of the ocean to 12.8 TmolSi yr^{-1}, which accounts for a previously ignored sink that is necessary to adequately assess the global balance of the marine Si cycle.

The biogeochemical cycle of silicon (Si) interacts with relevant marine chemical and ecological processes, which include modulation of the primary production[1] and removal of atmospheric CO_2 (ref. [2]). It also intertwines with the cycling of carbon, nitrogen, phosphorus, iron, radium, barium and germanium. Consequently, there is interest in quantifying the 'journey of Si' through the world's oceans and understanding the forces that govern it. The conceptualization of the marine Si cycle has revolved around two initial assumptions that have been transferred historically from one biogeochemical model to another over the years[1,3–7]. First, Si is recirculated in the ocean essentially through its utilization by planktonic diatoms, which consume silicic acid (that is, dissolved silica (DSi)) to elaborate a skeleton of biogenic silica (BSi), but other Si-consuming organisms (sponges, radiolarians, silicoflagellates, choanoflagellates and so on) would make negligible contributions. Second, the biogeochemical cycle is at a steady state, being the annual Si output from the ocean—essentially thought to occur by burial of BSi in sediments—compensated by an equivalent Si inflow as DSi. Recent discoveries challenge both long-standing assumptions.

Between 2009 and 2019, several revisions[7–12] of the mechanisms that bring DSi into the ocean increased the net input flux ($F_{C(net)}$) from 6.1 TmolSi yr^{-1} (a value set in 1995[6]) to 12.1 TmolSi yr^{-1}. In contrast, the estimated Si outflow ($F_{B(net)}$) remained at 6.3 TmolSi yr^{-1} for most of that period[13], which throws the cycle into a large positive imbalance. In 2017, a major Si sink—not strictly biological—was identified after discovering that 57–75% of the non-refractory BSi deposited in the sediments of warm continental margins readily becomes authigenic siliceous clay by reverse weathering[11] and buries 4.5–4.9 TmolSi yr^{-1}. This new sink reduced considerably the imbalance of the cycle budget, but a gap of +1.1 TmolSi yr^{-1} still persisted.

In this regard, several studies reported that siliceous sponges may also operate as Si sinks[14–18]. Their historical omission from the global cycle budget derives from the fact that to quantify sponges as a Si sink is difficult and, unlike recently suggested[8], far more complex than merely dealing with only their DSi consumption. The longevity of sponges can range from decades to millenia[14,16,17,19,20]. Thus, the Si consumed within a year will accumulate as BSi standing crop (that is, skeletal growth) for a variable long period in each living sponge, which largely decouples the annual rate of Si consumption from that of Si deposition to the sediment. Additionally, an unknown part of the deposited skeletons after sponge death will dissolve as DSi before and during early burial and will not qualify as Si output. Thus, the connection between sponge DSi consumption and BSi burial is not straightforward. A suitable way to assess the role of sponges as a Si sink is to quantify the rate at which their BSi is definitively buried in the sediments, a flux not approached so far.

Currently, the reservoirs of BSi in marine sediments are believed to consist fundamentally of diatom BSi (frustules)[6–8]. Diatoms consume concomitantly inorganic carbon (that is, CO_2) through their photosynthesis and DSi through their frustule growth, which connects stoichiometrically the production of organic carbon and that of BSi. Here we show that siliceous skeletons from sponges and radiolarians—which represent BSi produced without association to a photosynthetic generation of organic carbon and can be defined as 'dark' BSi—dominate and co-dominate in many marine sediments. Much of this dark BSi has passed unnoticed in routine quantifications of the total BSi because it is relatively refractory. The oversight affects the current understanding of the equilibrium between Si inputs and outputs in the marine biogeochemical Si cycle.

Refractory BSi neglected in sediments

There are a variety of methods to estimate the total BSi content in sediments, but wet alkaline digestions emerge as overwhelmingly preferred for their versatility and simplicity. For marine sediments, digestion in 1% sodium carbonate at 85 °C for five hours is the common procedure, following the DeMaster's technique[5]. Digestions

[1]Center for Advanced Studies of Blanes (CEAB), Spanish National Research Council (CSIC), Girona, Spain. [2]Institute of Marine Sciences (ICM-CSIC), Barcelona, Spain. [3]University of Brest, CNRS, LEMAR, Plouzané, France. *e-mail: maldonado@ceab.csic.es

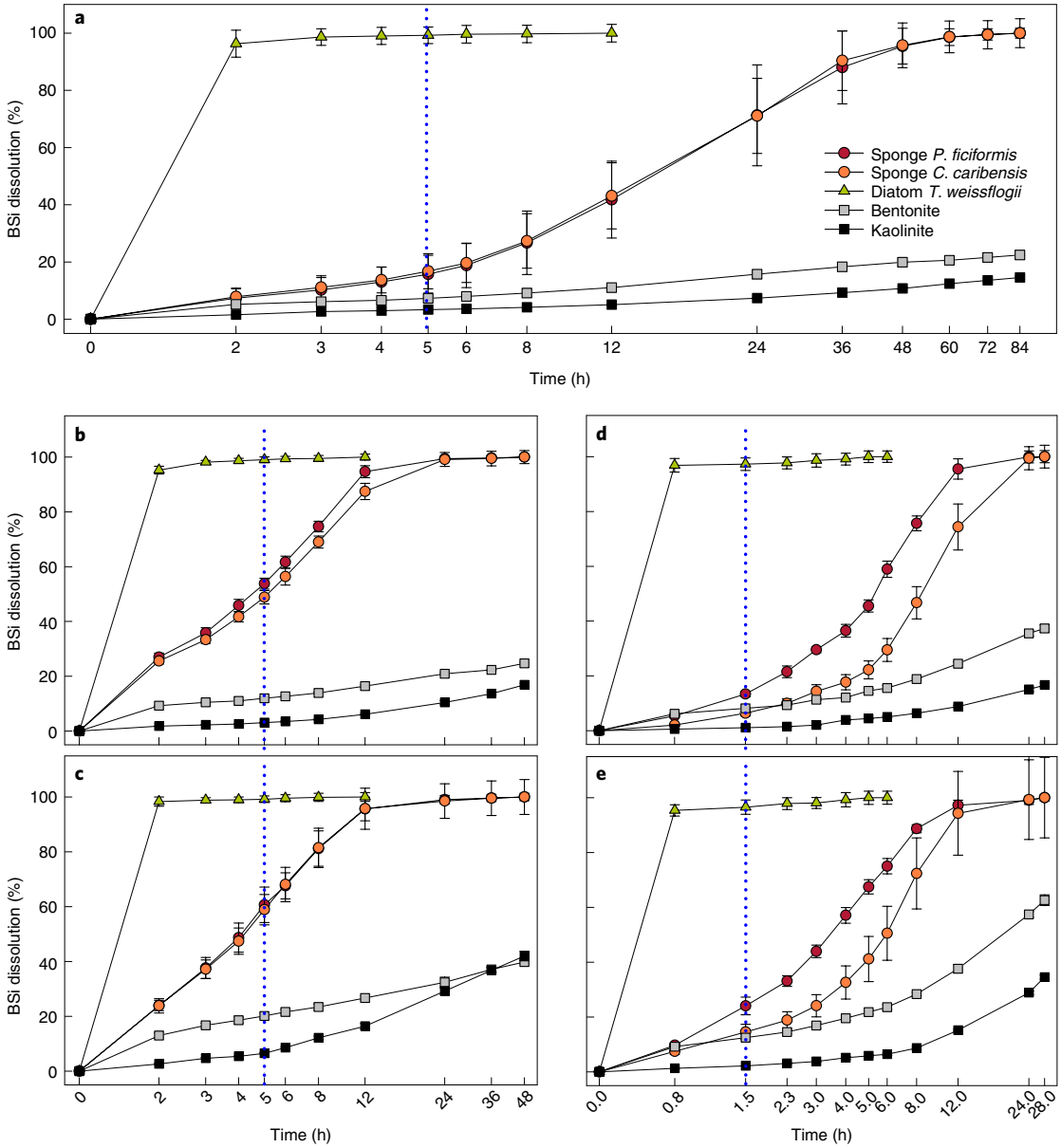

Fig. 1 | Digestion kinetics of BSi and LSi pure materials. a–e, Comparative dissolution kinetics of frustules of cultured *Thalassiosira weissflogii*, needle-like spicules of the sponge *Petrosia ficiformis*, star-like spicules of the sponge *Chondrilla caribensis*, bentonite and kaolinite in 1% (ref. [5]) (**a**), 5% (ref. [21]) (**b**) and 22% (ref. [23]) (**c**) sodium carbonate at 85 °C, as well as in 0.2 M (ref. [25]) (**d**) and 0.5 M (ref. [26]) (**e**) sodium hydroxide at 85 °C. Symbols represent the average dissolution (%) and error bars are the s.d. values calculated from eight replicates. Time (h) is shown as a logarithmic scale. The blue dotted vertical lines refer to the recommended digestion time for each technique.

based on stronger (5% and 22%) sodium carbonate solutions have also been proposed[21–23]. Terrestrial soils, but rarely marine sediments, are processed with even more aggressive solvents (0.1–0.5 M sodium hydroxide at 85–100 °C for two hours[24–26]). Here we show that, whereas the various digestion methods efficiently retrieve the amount of diatom BSi, they do not work for sponge BSi (Figs. 1 and 2). The comparative digestion of (1) two types of sponge spicules with different surface area, (2) frustules of cultured diatoms and (3) two forms of lithogenic silica (LSi) represented by kaolinite and bentonite aluminosilicates (Methods and Supplementary Table 1) revealed major differences in dissolution dynamics. The 1% sodium carbonate approach dissolved 100% of diatom BSi at the recommended digestion time (five hours)[5,27]. In stark contrast, during that digestion time, less than 16.2 ± 6.2% of sponge BSi was dissolved (Fig. 1a), irrespective of obvious specific surface area differences between the sponge spicule types (Fig. 2). Scanning electron microscopy (SEM) after five hours of digestion documented that diatom frustules were dissolved completely, whereas this digestion caused only a very incipient dissolution of the surface of the silica in the two types of assayed spicules (Fig. 2). Complete dissolution of the sponge BSi required over 60 hours, whereas most frustules of the assayed diatom had digested entirely after only 2–3 hours (Fig. 1a). To routinely accomplish a 60 hour digestion for sponge BSi is unpractical because a significant amount of the LSi that typically occurs in the sediments will also be dissolved (Fig. 1a), favouring an overestimation of BSi contents.

More aggressive alkaline digestions in either sodium carbonate (5% and 22%) or sodium hydroxide (0.2 and 0.5 M) did not improve the sponge BSi detection (Fig. 1b–e): by the time of complete frustule digestion, the sponge skeletons were only dissolved partially, and, by

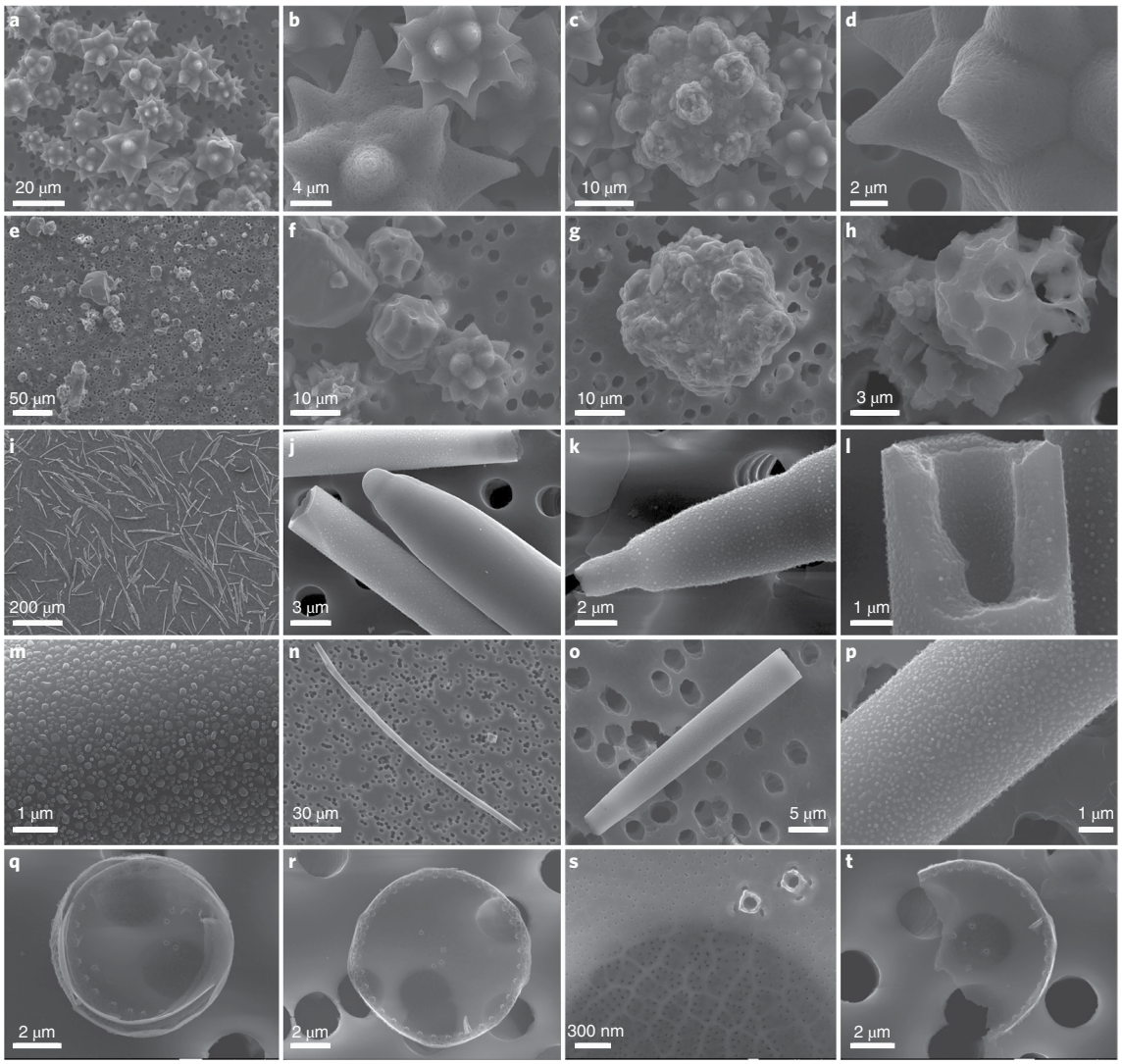

Fig. 2 | Diatom and sponge BSi skeletons during digestion in 1% sodium carbonate at 85 °C. a–d, The star-like spicules of the sponge *C. caribensis* after 5 h of digestion show that the bulk of the spicules remain undigested (**a**) and that only superficial erosion is attained (**b** and **c**), which causes tiny pits (**c** and **d**). **e–h**, Spicules of *C. caribensis* after 48 h of digestion. Most of the stars remain as fragments (**e**) that can no longer be recognized as spicules, except for few cases (**f**). Yet a good portion of the initial sponge BSi remains undigested even after 48 h of treatment (**g** and **h**). **i–m**, The needle-like spicules of *P. ficiformis* after 5 h of digestion show that most spicules remain undigested (**i** and **j**). Increased magnification (**k** and **l**) shows that only the silica surface of the spicules is eroded and reveals a granulated pattern that recalls the silica nanospherules (**m**) formed within the silicification vesicle of the sponge cells during the early silicification steps. **n–p**, The spicules of *P. ficiformis* after 48 h of digestion show that fewer recognizable spicules (**n**) and fragments (**o**) remain. Again, the progressive digestion of the silica reveals a nanospherule pattern (**p**). **q–t**, Frustules of *T. weissflogii* after 2 h of digestion. Most of the diatoms are entirely dissolved, being no longer detectable. Yet some complete frustules can be found, although their walls are so thin that they become translucent to the electron beam of the SEM, which reveals the porous pattern of the 3 µm pore filter on which the frustules rest (**q–t**). The delicate ornamentation of the frustules is still visible at high magnification (**s**).

the time of complete digestion of the sponge skeletons, much of the LSi was also dissolved. Indeed, extended or very aggressive digestions of marine sediments are systematically avoided in routine BSi determinations to circumvent laborious aluminium (Al)-based corrections for LSi contamination[21,24,28]. Additionally, the particles of sponge BSi that remained after the primary sediment digestion will erroneously be accounted as LSi by any subsequent digestion, which biases the actual Al:Si ratio of aluminosilicates, a parameter, in turn, required to correct the BSi determination[24].

The concluding message is that the most widely used method to determine the total BSi in sediments (1% Na_2CO_3) overlooks more than 80% of the sponge BSi and that the alternative digestion protocols also work inefficiently.

Quantifying dark BSi in sediments

The resistance of sponge BSi to digestion in 1% Na_2CO_3 was suspected by DeMaster when he first proposed the method in 1981[5]. Nevertheless, under the widespread supposition that the contribution of sponges to BSi in marine sediments was 'insignificant'[5,7,29], the importance of overlooking much of the sponge BSi was assumed by the users of the method as an inaccuracy 'smaller than insignificant'. Our results here indicate that such a presumption is erroneous.

We quantified the relative contribution of diatoms, sponges, radiolarians and silicoflagellates to total BSi in the 1 cm thick uppermost layer of 17 marine sediment cores. The cores, collected from depths of 3 to 5,204 m, represent an array of depositional environments, which includes continental shelves, slopes, rises, plateaus,

seamounts and basin bottoms from different oceans and seas (Supplementary Information (Discussion 1), Supplementary Fig. 1 and Supplementary Table 2).

Light microscopy, digital photography and morphometric software were used to measure the volume (and then the Si mass) of every recognizable sponge spicule, radiolarian and silicoflagellate, either complete or broken. A total of 102,197 spicules, either entire (9.7%) or as fragments (90.3%), as well as 50,183 radiolarians or their fragments and 11,488 silicoflagellates, were processed over five years of microscopy study (Supplementary Fig. 2). The BSi contribution of diatoms was estimated from the total BSi content yielded by the 1% sodium carbonate method after discounting the contribution owing to the dissolution (16.2%) of sponge spicules and assuming radiolarians as negligible (Methods). The results revealed that the relative contribution of sponge BSi to total BSi was substantial (29.3–99.7%) in 8 of the 17 cores (Fig. 3). These sediments came from continental shelves (cores 3, 5 and 7), slopes (cores 14 and 15) and seamounts (cores 2, 4 and 6). Only one continental shelf environment—the distal-shelf facies of the Gulf of Cadiz (core 10)—was poor (3.9%) in sponge BSi.

The highest sponge BSi contribution occurred in core 4 (a North Atlantic seamount that hosts sponge aggregations[30]), in which spicules represented over 99% of the total BSi. Sponge BSi also contributed 95.9 and 81.7% in cores 7 and 6 (Fig. 3), respectively, collected from a Mediterranean seagrass meadow and from the base of a seamount (Galicia Bank) at the Northeastern Atlantic margin. Spicules were also important (62.8%) at the bathyal slope of the Great Barrier Reef in the Pacific Ocean (core 15). In four other cores (2, 3, 5 and 14) that represent continental slopes and shelves from the North Atlantic and Indian Oceans, sponge BSi was still substantial (29.3–48.6%).

In absolute terms (Fig. 3 and Supplementary Table 3), the largest sponge BSi value (76.31 ± 38.15 mgSi g^{-1}) occurred in core 4 from Flemish Cap, collected within a *Geodia* spp. ground[30], one of the many sponge aggregations that occur over the world's ocean[31]. The slope of the Bransfield Strait in Antarctica (core 17), another ocean region in which sponge aggregations abound[32–34], ranked second in absolute values of sponge BSi, with 2.57 ± 0.86 mgSi g^{-1}. However, in this Antarctic sediment, sponge spicules represented only 5.3% of the total BSi, which was dominated by diatoms (45.69 ± 2.32 mgSi g^{-1}). Frustules were even more abundant (98.56 ± 8.53 mgSi g^{-1}) in core 16, from a Southern Ocean siliceous-ooze area[35], in which sponge spicules were very rare (0.13%). In summary, in most sediments from relatively open-water environments, such as the Girona continental rise (core 8), central basins (cores 9, 11–13 and 16) and slope basins (core 1), the sponge BSi contribution was comparatively small (<25%).

Silicifiers other than diatoms and sponges always contributed marginally. Siliceous radiolarians were regularly detected in ten cores (1, 2, 4–6, 10 and 14–17), but did not represent much of the total BSi (Fig. 3 and Supplementary Table 3). Radiolarian BSi reached its maximum (5.94 ± 1.30 mgSi g^{-1}) in the Southern Ocean biosiliceous ooze (core 16), in agreement with previous knowledge that reported patches of abundant radiolarian skeletons scattered across this and other ocean areas[35–37]. Nevertheless, that Southern Ocean BSi-rich (104.80 mgSi g^{-1}) sediment was dominated by frustules (94.1%), with radiolarians contributing only 5.7% of the total BSi. Silicoflagellates were even less important globally, not being retrieved in the uppermost sediments of most cores. Their best representation occurred in Southern Ocean cores, although their maximum contribution (0.17% in core 16) was still insignificant (Supplementary Table 3).

These results indicate that, unlike traditionally hypothesized, a significant portion of the BSi at the superficial sediment layer of continental margins and around seamounts comes from sponges, and not only from diatoms (Supplementary Information (Discussion 2)).

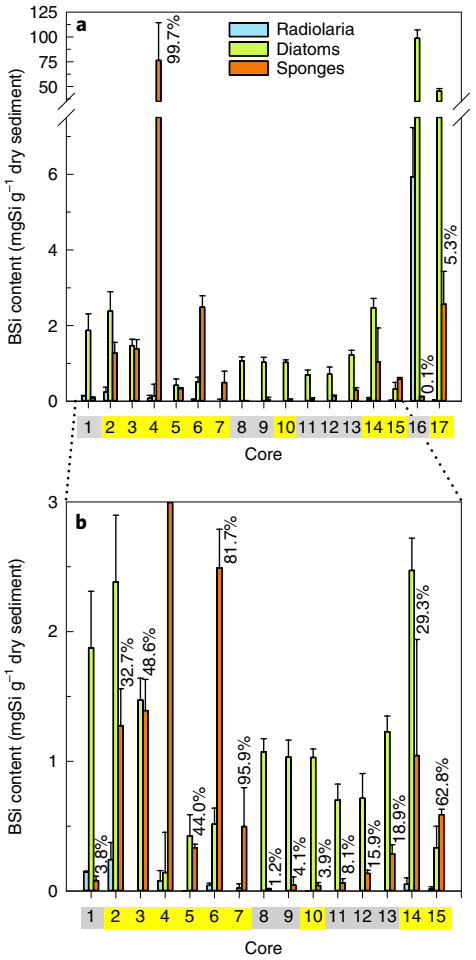

Fig. 3 | Contributors of BSi in superficial sediments. a, Mean (±s.d.) content of BSi from diatoms, sponges and radiolarians in the 1 cm thick uppermost layer of sediment of each of the 17 studied cores. **b**, The graph with BSi contents lower than 3 mgSi g^{-1} (except core 4) makes visible the minor contributions of some BSi types into some cores. Percentages above the orange bars indicate the relative contribution of sponge BSi to total BSi in the sediments (absolute values are given in Supplementary Table 3). The sponge BSi contribution was substantial (29–99%) in cores from continental margins and around seamounts (core numbers with a yellow background). Diatom BSi dominated the remaining cores, mostly collected below open waters in ocean basins (core numbers with a grey background).

Preservation of dark BSi

The low solubility of sponge BSi has enabled such a Si reservoir to pass unnoticed in routine digestions to quantify the total BSi in marine sediments. The question arises now as to whether the omission may have led to a substantial underestimate of the Si burial in the global oceans.

In practical terms, the BSi deposited at the sediments continues to dissolve during its burial until a saturating silicate concentration is reached in the interstitial water. This typically happens no deeper than 30–35 cm in the sediments[8,21,38]. To be conservative, we regarded that BSi preservation starts not at a 30 cm burial depth but at 50 cm. The sponge BSi preservation was then quantified in each core as the difference (%) in sponge BSi content between the 1 cm thick upper sediment layer and that buried at 50 cm, after assuming an approximately constant rate of sponge BSi deposition (Methods). In our cores, sponge BSi preservation ranged from 10.8 to 84.9% (Table 1). Overrated preservation (>100%) resulted in four cores: the Bay of Brest (core 3), the turbiditic Girona rise (core 8), the

Table 1 | Preservation (%) of sponge and radiolarian BSi

		Burial depth		Preservation of Si (%)	Corrected preservation of Si (%)
		0 cm	50 cm		
CORE 1	Age (kyr)	0.00	8.75		
	Sponges	79.54 ± 33.84	52.28 ± 2.05	65.7	65.7
	Radiolaria	147.56 ± 5.28	42.29 ± 6.56	28.7	28.7
CORE 2	Age (kyr)	12.00	14.18		
	Sponges	1,275.07 ± 284.27	225.08 ± 23.27	17.7	17.7
	Radiolaria	241.96 ± 131.72	8.90 ± 5.78	3.7	3.7
CORE 3	Age (kyr)	0.00	0.94		
	Sponges	1,390.63 ± 240.80	3,608.75 ± 323.77	259.5	45.2
CORE 4	Age (kyr)	0.00	9.94		
	Sponges	76,313.84 ± 38,146.98	8,222.38 ± 1,044.38	10.8	10.8
	Radiolaria	78.35 ± 79.26	0.14 ± 0.24	0.2	0.2
CORE 5	Age (kyr)	0.00	0.77		
	Sponges	334.27 ± 26.01	116.85 ± 37.73	35.0	35.0
	Radiolaria	1.09 ± 0.36	0.09 ± 0.12	8.1	8.1
CORE 6	Age (kyr)	0.00	14.74		
	Sponges	2,491.22 ± 297.36	860.91 ± 258.47	34.6	34.6
	Radiolaria	42.39 ± 16.88	2.26 ± 2.37	5.3	5.3
CORE 7	Age (kyr)	0.00	0.47		
	Sponges	496.31 ± 300.36	188.46 ± 22.25	38.0	38.0
CORE 8	Age (kyr)	0.00	6.39		
	Sponges	12.50 ± 6.64	15.50 ± 15.92	124.0	45.2
CORE 9	Age (kyr)	0.00	1.22		
	Sponges	44.56 ± 63.82	7.08 ± 9.08	15.9	15.9
CORE 10	Age (kyr)	0.00	2.21		
	Sponges	42.27 ± 22.74	35.59 ± 27.24	84.2	84.2
	Radiolaria	0.05 ± 0.09	0.94 ± 1.63	1870.8	6.8
CORE 11	Age (kyr)	0.00	4.17		
	Sponges	61.49 ± 33.60	52.17 ± 49.35	84.9	84.9
CORE 12	Age (kyr)	0.00	74.07		
	Sponges	134.72 ± 25.94	78.30 ± 9.00	58.1	58.1
CORE 13	Age (kyr)	0.00	8.47		
	Sponges	286.99 ± 69.43	105.36 ± 5.45	36.7	36.7
CORE 14	Age (kyr)	0.00	1.66		
	Sponges	1,043.74 ± 895.74	222.25 ± 13.46	21.3	2
	Radiolaria	50.87 ± 50.03	0.62 ± 0.15	1.2	1.2
CORE 15	Age (kyr)	0.00	3.64		
	Sponges	587.40 ± 42.45	498.95 ± 54.04	84.9	84.9
	Radiolaria	14.73 ± 17.91	0.03 ± 0.05	0.2	0.2
CORE 16	Age (kyr)	0.00	7.24		
	Sponges	125.50 ± 3.03	171.84 ± 60.99	136.9	45.2
	Radiolaria	5,935.55 ± 1,300.70	7,382.34 ± 1,765.71	124.4	6.8
CORE 17	Age (kyr)	0.00	0.50		
	Sponges	2,572.09 ± 861.21	2,894.33 ± 513.81	112.5	45.2
	Radiolaria	26.22 ± 9.67	53.33 ± 3.40	203.4	6.8

Estimated from the difference in BSi content (μgSi g^{-1} sed) between the superficial sediment and that buried at 50 cm. Sediment age at 50 cm is given. Overrated preservation (>100%) resulted in some cores (Supplementary Information (Discussion 3)), which were not considered when calculating average preservation (%) for sponge and radiolarian BSi. Subsequent calculations that involved overrated cores conservatively assumed a 'corrected preservation' identical to the average that resulted from the pool of the remaining cores.

Southern Ocean biosiliceous oozes (core 16) and the Antarctic slope (core 17), and these were not considered when calculating the average BSi preservation (Supplementary Information (Discussion 3)). Not to overestimate in subsequent calculations, it was assumed that the preservation in each of the overrated cores could not be higher than the average value that resulted from the 13 remaining

Table 2 | Age, wet bulk density and deposition rate of the sediment, along with content and burial rate of BSi at 50 cm, in the different cores

Core	Age at 50 cm (yr)	Sediment density ($g\,cm^{-3}$)	Deposition rate ($g\,sed\,m^{-2}\,yr^{-1}$)	Sponge BSi at 50 cm ($\mu gSi\,g^{-1}$)	Sponge BSi burial rate ($mgSi\,m^{-2}\,yr^{-1}$)	Radiolarian BSi at 50 cm ($\mu gSi\,g^{-1}$)	Radiolarian BSi burial rate ($mgSi\,m^{-2}\,yr^{-1}$)
1	8,754	1.557	88.915	52.277	4.648	42.285	3.760
2	2,182	1.601	366.824	225.082	82.566	8.901	3.265
3	944	1.659	879.051	628.600	552.571	-	-
4	9,937	1.618	81.396	8,222.379	669.271	0.137	0.011
5	767	1.652	1,077.287	116.852	125.883	0.089	0.095
6	14,741	1.552	52.641	860.915	45.319	2.263	0.119
7	471	1.660	1,763.031	188.459	332.260	-	-
8	6,390	1.563	122.309	5.649	0.691	-	-
9	1,217	1.554	638.807	7.079	4.522	-	-
10	2,212	1.654	373.797	35.587	13.302	0.003	0.001
11	4,170	1.586	190.157	52.172	9.921	-	-
12	74,074	1.441	9.728	78.295	0.762	-	-
13	8,475	1.418	83.680	105.364	8.817	-	-
14	1,661	1.464	440.747	222.253	97.957	0.616	0.272
15	3,643	1.604	220.143	498.947	109.840	0.032	0.007
16	7,236	1.395	96.365	56.728	5.467	402.017	38.740
17	500	1.615	1,615.018	1,162.650	1,877.701	1.776	2.868

The amount of BSi preserved at 50 cm burial depth (considering corrected BSi preservation for sponges in cores 3, 8, 16 and 17 and for radiolarians in cores 10, 16 and 17) and the derived BSi burial rates for sponges and radiolarians. The continental-margin–seamounts compartment is represented by cores 2–7, 10, 14, 15 and 17. The basin compartment is represented by cores 1, 8, 9, 11–13 and 16.

ones (Table 1). Such a 'correction' is conservative because an averaged preservation is applied to sediments of the Southern Ocean (cores 16 and 17) and the Bay of Brest (core 3), which are known to be characterized by a greater preservation than the average in marine sediments[39,40].

Calculations yielded a global average preservation of $45.2 \pm 27.4\%$ for sponge BSi and $6.8 \pm 10.1\%$ for radiolarian BSi. Diatom BSi preservation, estimated from the literature[8], is 8%. The comparison of these three values indicates that sponge BSi has a great potential for Si burial (Supplementary Figs. 2 and 3).

Burial flux of dark BSi

The global burial flux of sponge and radiolarian BSi is quantified herein. Ocean extension was calculated[41] at $361.88 \times 10^6\,km^2$ (Methods). As we noticed marked differences between 'basin-rise environments' and 'continental-margin–seamount environments' regarding sponge BSi content in sediments, the ocean was simplified to those main compartments, where basins and rises represent 70.2% of the seafloor. The remaining 29.8% consists of an assemblage of continental margins plus seamounts, plateaus and other minor geomorphological features. The continental-margin–seamount compartment is represented by ten cores and the basin compartment by seven (Fig. 3, Supplementary Information (Discussion 1) and Supplementary Table 2). We then estimated the age of the sediments at 50 cm, wet bulk density of the sediments and the amount of sponge BSi preserved at 50 cm (Table 2 and Methods). By combining all four of these parameters, the amount of sponge BSi buried per metre squared and year was finally calculated for each core (Table 2). The mean rates of sponge BSi burial spanned two orders of magnitude across cores of the continental-margin–seamount compartment, from $13.3\,mgSi\,m^{-2}\,yr^{-1}$ at the deep continental shelf of the Gulf of Cadiz (core 10) to $1{,}877.7\,mgSi\,m^{-2}\,yr^{-1}$ at the Antarctic slope (core 17). The span illustrates the large sampled variety of depositional environments (Supplementary Information (Discussion 3)). In the basin compartment, sponge BSi preservation reflects the relatively homogeneous depositional scenario expected for distal-margin and open-water environments, with low rates varying minimally across five of the seven cores ($4.5–9.9\,mgSi\,m^{-2}\,yr^{-1}$). The preservation of sponge BSi was even lower at the Western Mediterranean continental rise (core 8) and the Pacific Clarion–Clipperton fracture zone (core 12), being respectively 0.7 and $0.8\,mgSi\,m^{-2}\,yr^{-1}$. Unlike that known for planktonic diatoms, the burial rate of sponge BSi barely correlates with the sediment deposition rate (Supplementary Fig. 4a). The non-planktonic nature of the sponge BSi production disrupts the relationship (Supplementary Information (Discussion 3)). Neither did sponge BSi preservation (%) correlate with total BSi in the sediments (Supplementary Fig. 4b), because of the general resistance of spicules to dissolution (Supplementary Information (Discussion 3)).

The approach used for sponge BSi was also extended to radiolarian BSi. Siliceous radiolarians occurred in only 10 of the 17 cores, with estimated burial rates from 0.1×10^{-2} to $38.7\,mgSi\,m^{-2}\,yr^{-1}$, and preservation percentages varying from 0.2 to 28.7% (Tables 1 and 2). As in the case of sponge BSi, overrated radiolarian preservation in the Southern Ocean sediments (cores 16 and 17) had to be adjusted down to the global average ($6.8 \pm 10.1\%$), as well as in core 10 (Supplementary Information (Discussion 3)).

The global burial flux for the sponge and radiolarian BSi in the ocean was then estimated by multiplying the preservation rates across the extension of the pertinent ocean compartments for each organism type (Table 3). For sponge BSi, the extensions of the continental-margin–seamount and basin-rise compartments were calculated and the mean BSi burial rate that resulted from the corresponding set of associated cores applied (Methods). Yet, sponge aggregations occur in basins of all oceans[31], but their potential BSi contribution was not incorporated in the set of 'basin cores' because samples of abyssal sponge grounds are lacking in the repositories. Evidence from both the literature[33,42,43] and cores 4, 5 and 17, which represent aggregations on continental margins, suggests that the sponge BSi content in the sediments of aggregations

Table 3 | Preservation rates and burial fluxes for dark BSi through sponges and radiolarian skeletons in their ocean compartments

Ocean compartment	Compartment extension ($km^2 \times 10^6$)	Sponge BSi preservation ($mgSi\,m^{-2}\,yr^{-1}$)	Sponge BSi burial flux ($TmolSi\,yr^{-1}$)	Radiolarian BSi preservation ($mgSi\,m^{-2}\,yr^{-1}$)	Radiolarian BSi burial flux ($TmolSi\,yr^{-1}$)	Total BSi burial flux ($TmolSi\,yr^{-1}$)
Margins and seamounts	108.02	390.667 ± 568.601	1.503 ± 2.187	-	-	-
Basins without aggregations	248.78	4.975 ± 3.556	0.044 ± 0.032	-	-	-
Aggregations in basins	5.08	890.952 ± 896.701	0.161 ± 0.162	-	-	-
Basins and 2% aggregations	253.86	22.695 ± 124.664	0.205 ± 0.143	-	-	-
Radiolarian oozes	5.34	-	-	38.740 ± 8.489	0.007 ± 0.002	-
Radiolarian-rich diatom oozes	19.46	-	-	38.740 ± 8.489	0.027 ± 0.006	-
Rest of 'radiolarian' ocean	337.08	-	-	4.914 ± 11.984	0.059 ± 0.104	-
Global ocean	361.88	-	1.708 ± 1.611	-	0.093 ± 0.051	1.801 ± 1.396

For sponges, the ocean seafloor was divided into two compartments, 'continental margins, seamounts and minor additional geomorphological features' versus 'ocean basins and rises', with about 2% of abyssal (or deeper) basin bottoms estimated to contain sponge aggregations. For radiolarians, the ocean floor was divided into three major compartments: radiolarian oozes, radiolarian-rich diatom oozes (that is, sediment dominated by diatom frustules but still rich in siliceous radiolarian testa) and the rest of the ocean (Supplementary Fig. 5).

may be orders of magnitude higher than those in sponge-lacking areas. To address the lack of representability of sponge grounds in basin cores, we assumed that about 2% of the seafloor in basins and rises hosts sponge aggregations. Such an assumption is thought to be conservative. Observations and predictive modelling on the occurrence of sponge grounds between 200 and 5,000 m in the North Atlantic—the best-studied ocean area in this regard—suggest a global occupancy much larger than 2%, with sponge grounds that extend over 33.5% of the Exclusive Economic Zone and High Seas in Greenland, 25.5% in Norway, 14.8% in Iceland, 10.5% in the Faeroes, 5.6% in Canada and so on[44]. Therefore, to consider the effects of sponge aggregations in basins (Table 3), we applied the average burial rate ($890.9 \pm 896.7\,mg\ Si\,m^{-2}\,yr^{-1}$) that results from the three cores that involve sponge aggregations (cores 4, 5 and 17). The final calculations yielded a global burial flux through sponge BSi of $1.7 \pm 1.6\,TmolSi\,yr^{-1}$ (Table 3). Note that error propagation incorporating the marked differences in the BSi burial rate across cores from very different environments in the world's oceans leads to a large s.d. value.

We applied the same reasoning to radiolarian BSi, but considered the ocean compartments for these planktonic organisms to be different from those defined for sponges (Table 3). A recent mapping of the seafloor sediments[36] identified many small areas across the ocean seafloor characterized by the abundance of radiolarian skeletons in the sediments (oozes). By importing into ArcGis Software the available map layers, we determined that radiolarian oozes consist of a total of 64 patches with a global extension of $5.3 \times 10^6\,km^2$ and that radiolarian-rich diatom oozes occupied $19.5 \times 10^6\,km^2$, mostly in the Southern Ocean (Supplementary Fig. 5). To those extensions, the BSi content and preservation values of core 16, which testified for radiolarian abundance in the oozes (Fig. 3), were applied (Table 3). For the rest of the ocean, the average that results from all cores, core 16 included, was used. This was done to incorporate the notion that additional patches of radiolarian oozes occur, though not yet identified[36]. The global calculations yielded a burial flux through radiolarian BSi of $9.3 \pm 5.1 \times 10^{-2}\,TmolSi\,yr^{-1}$, that is, two orders of magnitude lower than that of sponge BSi. Yet, these calculations for radiolarian BSi must be seen as a first conservative attempt to set the global magnitude of the burial flux. Subsequent readjustments based on the empirical determination of local preservation values may be required to relax our very conservative scenario that radiolarian BSi preservation in the oozes is only 6.8% (Supplementary Information (Discussion 3) and Supplementary Table 4).

Collectively, the burial of dark BSi, quantified herein through sponge and radiolarian skeletons, increases by 28.6% the previous value of the biological Si sink ($6.3 \pm 3.6\,TmolSi\,yr^{-1}$), which considered only diatoms. Sponge BSi accounts for 94.8% of that increase, with a minor (5.2%) global contribution from radiolarians. The identified Si sink through dark BSi ($-1.8 \pm 1.4\,TmolSi\,yr^{-1}$) rises the global output flux to $12.8\,TmolSi\,yr^{-1}$ and brings the ocean budget close to equilibrium, but now with a subtle negative imbalance ($-0.7\,TmolSi\,yr^{-1}$). Such a small gap is likely to be filled readily, because recent studies have reported small, local Si inputs into the ocean through DSi-rich ground water[10,45–47], which await quantification.

Online content

Any methods, additional references, Nature Research reporting summaries, source data, statements of code and data availability and associated accession codes are available at https://doi.org/10.1038/s41561-019-0430-7.

Received: 2 February 2018; Accepted: 17 July 2019;
Published online: 26 August 2019

References

1. Nelson, D. M., Tréguer, P., Brzezinski, M. A., Leynaert, A. & Quéguiner, B. Production and dissolution of biogenic silica in the ocean: revised global estimates, comparison with regional data and relationship to biogenic sedimentation. *Glob. Biogeochem. Cycles* **9**, 359–372 (1995).
2. Tréguer, P. & Pondaven, P. Silica control of carbon dioxide. *Nature* **406**, 358–359 (2000).
3. Harriss, R. C. Biological buffering of oceanic silica. *Nature* **212**, 275–276 (1966).
4. Calvert, S. E. Silica balance in the ocean and diagenesis. *Nature* **219**, 919–920 (1968).
5. DeMaster, D. J. The supply and accumulation of silica in the marine environment. *Geochim. Cosmochim. Acta* **45**, 1715–1732 (1981).
6. Tréguer, P. et al. The silica balance in the world ocean: a reestimate. *Science* **268**, 375–379 (1995).
7. Laruelle, G. G. et al. Anthropogenic perturbations of the silicon cycle at the global scale: key role of the land-ocean transition. *Glob. Biogeochem. Cycles* **23**, GB4031 (2009).

8. Tréguer, P. J., De La & Rocha, C. L. The world ocean silica cycle. *Ann. Rev. Mar. Sci.* **5**, 477–501 (2013).
9. Frings, P. J., Clymans, W., Fontorbe, G., De La Rocha, C. & Conley, D. J. The continental Si cycle and its impact on the ocean Si isotope budget. *Chem. Geol.* **425**, 12–36 (2017).
10. Hawkings, J. R. et al. Ice sheets as a missing source of silica to the polar oceans. *Nat. Commun.* **8**, 14198 (2017).
11. Rahman, S., Aller, R. C. & Cochran, J. K. The missing silica sink: revisiting the marine sedimentary Si cycle using cosmogenic ^{32}Si. *Glob. Biogeochem. Cycles* **31**, 1559–1578 (2017).
12. Rahman, S., Tamborski, J. J., Charette, M. A. & Cochran, J. K. Dissolved silica in the subterranean estuary and the impact of submarine groundwater discharge on the global marine silica budget. *Mar. Chem.* **208**, 29–42 (2019).
13. Tréguer, P. J. The Southern Ocean silica cycle. *C. R. Geosci.* **346**, 279–286 (2014).
14. Maldonado, M. et al. Siliceous sponges as a silicon sink: an overlooked aspect of the benthopelagic coupling in the marine silicon cycle. *Limnol. Oceanogr.* **50**, 799–809 (2005).
15. Maldonado, M., Navarro, L., Grasa, A., Gonzalez, A. & Vaquerizo, I. Silicon uptake by sponges: a twist to understanding nutrient cycling on continental margins. *Sci. Rep.* **1**, 30 (2011).
16. Maldonado, M., Riesgo, A., Bucci, A. & Rützler, K. Revisiting silicon budgets at a tropical continental shelf: silica standing stocks in sponges surpass those in diatoms. *Limnol. Oceanogr.* **55**, 2001–2010 (2010).
17. Maldonado, M., Ribes, M. & Van Duyl, F. C. Nutrient fluxes through sponges: biology, budgets, and ecological implications. *Adv. Mar. Biol.* **62**, 114–182 (2012).
18. Chu, J. W. F., Maldonado, M., Yahel, G. & Leys, S. P. Glass sponge reefs as a silicon sink. *Mar. Ecol. Prog. Ser.* **441**, 1–14 (2011).
19. Jochum, K. P. et al. Whole-ocean changes in silica and Ge/Si ratios during the Last Deglacial deduced from long-lived giant glass sponges. *Geophys. Res. Lett.* **44**, 11,555–511,564 (2017).
20. Jochum, K. P., Wang, X., Vennemann, T. W., Sinha, B. & Müller, W. E. G. Siliceous deep-sea sponge *Monorhaphis chuni*: a potential paleoclimate archive in ancient animals. *Chem. Geol.* **300–301**, 143–151 (2012).
21. Hurd, D. C. Interactions of biogenic opal, sediment and seawater in the Central Equatorial Pacific. *Geochim. Cosmochim. Acta* **37**, 2257–2282 (1973).
22. Mortlock, R. A. & Froelich, P. N. A simple method for the rapid determination of biogenic opal in pelagic marine sediments. *Deep -Sea Res. I* **36**, 1415–1426 (1989).
23. Eggimann, D. W., Manheim, F. T. & Betzer, P. R. Dissolution and analysis of amorphous silica in marine sediments. *J. Sediment Petrol.* **50**, 215–225 (1980).
24. Kamatani, A. & Oku, O. Measuring biogenic silica in marine sediments. *Mar. Chem.* **68**, 219–229 (2000).
25. Paasche, E. Silicon and the ecology of marine plankton diatoms. II Silicate-uptake kinetics in five diatom species. *Mar. Biol.* **19**, 262–269 (1973).
26. Müller, P. J. & Schneider, R. An automated leaching method for the determination of opal in sediments and particulate matter. *Deep-Sea Res I* **40**, 425–444 (1993).
27. Conley, D. J. An interlaboratory comparison for the measurements of biogenic silica in sediments. *Mar. Chem.* **63**, 39–48 (1998).
28. Ragueneau, O. et al. A new method for the measurement of biogenic silica in suspended matter of coastal waters: using Si:Al ratios to correct for the mineral interference. *Cont. Shelf Res* **25**, 697–710 (2005).
29. Heinze C. in *The Silicon Cycle: Human Perturbations and Impacts on Aquatic Systems* (eds Ittekkot, V., Unger, D., Humborg, C. & An, N. T.) 229–244 (SCOPE Series Vol. 66, Island Press, 2006).
30. Murillo, F. J., Kenchington, E., Lawson, J. M., Li, G. & Piper, D. J. W. Ancient deep-sea sponge grounds on the Flemish Cap and Grand Bank, northwest Atlantic. *Mar. Biol.* **163**, 1–11 (2016).
31. Maldonado M., et al. in *Marine Animal Forests: The Ecology of Benthic Biodiversity Hotspots* (eds Rossi, S., Bramanti, L., Gori, A. & Orejas, C.) 145–183 (Springer International, 2017).
32. Dayton, P. K. Observations of growth, dispersal and population dynamics of some sponges in McMurdo Sound, Antarctica. *Colloq. Int. Cent. Natl Rech. Sci.* **291**, 271–282 (1979).
33. Gutt, J., Böhmer, A. & Dimmler, W. Antarctic sponge spicule mats shape macrobenthic diversity and act as a silicon trap. *Mar. Ecol. Prog. Ser.* **480**, 57–71 (2013).
34. Barthel, D. & Gutt, J. Sponge associations in the eastern Weddell Sea. *Antarct. Sci.* **4**, 137–150 (1992).
35. Lisitzin A. P. in *The Micropaleontology of Oceans* (eds Funnell, B. M. & Riedel W. R.) 173–195 (Cambridge Univ. Press, 1971).
36. Dutkiewicz, A., Müller, R. D., O'Callaghan, S. & Jónasson, H. Census of seafloor sediments in the world's ocean. *Geology* **43**, 795–798 (2016).
37. Boltovskoy, D., Kling, S. A., Takahashi, K. & Bjørklund, K. World atlas of distribution of recent Polycystina (Radiolaria). *Palaeontol. Electron.* **13**, 1–230 (2010).
38. Van Cappellen, P. & Qiu, L. Biogenic silica dissolution in sediments of the Southern Ocean. I. Solubility. *Deep-Sea Res II* **44**, 1109–1128 (1997).
39. DeMaster, D. J. The accumulation and cycling of biogenic silica in the Southern Ocean: revisiting the marine silica budget. *Deep-Sea Res II* **49**, 3155–3167 (2002).
40. Ragueneau, O. et al. Biodeposition by an invasive suspension feeder impacts the biogeochemical cycle of Si in a coastal ecosystem (Bay of Brest, France). *Biogeochemistry* **75**, 19–41 (2005).
41. Harris, P. T., Macmillan-Lawler, M., Rupp, J. & Baker, E. K. Geomorphology of the oceans. *Mar. Geol.* **352**, 4–24 (2014).
42. Bett, B. J. & Rice, A. L. The influence of hexactinellid sponge spicules on the patchy distribution of macrobenthos in the Porcupine Seabight (bathyal NE Atlantic). *Ophelia* **36**, 217–226 (1992).
43. Laguionie-Marchais, C., Kuhnz, L. A., Huffard, C. L., Ruhl, H. A. & Smith, K. L. Jr Spatial and temporal variation in sponge spicule patches at Station M, northeast Pacific. *Mar. Biol.* **162**, 617–624 (2015).
44. Howell, K.-L., Piechaud, N., Downie, A.-L. & Kenny, A. The distribution of deep-sea sponge aggregations in the North Atlantic and implications for their effective spatial management. *Deep-Sea Res I* **115**, 309–320 (2016).
45. Sospedra, J. et al. Identifying the main sources of silicate in coastal waters of the Southern Gulf of Valencia (Western Mediterranean Sea). *Oceanologia* **60**, 52–64 (2018).
46. Ehlert, C. et al. Transformation of silicon in a sandy beach ecosystem: insights from stable silicon isotopes from fresh and saline groundwaters. *Chem. Geol.* **440**, 207–218 (2016).
47. Lecher, A. Groundwater discharge in the Arctic: a review of studies and implications for biogeochemistry. *Hydrology* **4**, 41 (2017).

Acknowledgements

We thank the British Ocean Sediment Core Research Facility (BOSCORF-NOC) for providing access to cores 1, 12, 14 and 16. We also thank E. Kenchington, C. Campbell, K. Jarrett and J. Murillo (BIO) for making the data and sediment of cores 2 and 4 available. A. Ehrhold (IFREMER) is thanked for core 3, M. A. Mateo (CEAB) for core 7 and T. Whiteway (Australian Geosciences) for core 15. R. Ventosa and M. Abad are thanked for helping with the DSi autoanalyser determinations, B. Dursunkaya for helping with the digestion experiments and P. Talberg and L. Cross for providing strains of the *Thalassiossira* diatom. J. Krause is especially thanked for comments and insight on the manuscript. This study, which spanned five years, benefitted from funding by two grants of the Spanish MINECO (CTM2012-37787 and CTM2015-67221-R). Financial support by the European Union's Horizon 2020 research and innovation program to the SponGES project (grant agreement 679849) is acknowledged.

Author contributions

M.M. designed the study and experiments. Sediment and BSi digestions were conducted by M.M., M.L.A., C.S., M.G.-P. and C.G. Sediment cores were collected by G.E. Light microscopy determination of the BSi was conducted by M.L.A., C.S., M.G.-P. and C.G. under supervision of M.M. SEM and energy dispersive X-ray spectrometry analyses were conducted by M.M. and C.S. Data analyses were conducted by M.M. and M.L.A. and ArcGis mapping by M.G.-P. M.M. wrote the manuscript, with invaluable inputs made by M.L.A. and the rest of co-authors at different stages of the process.

Competing interests

The authors declare no competing interests.

Additional information

Supplementary information is available for this paper at https://doi.org/10.1038/s41561-019-0430-7.

Reprints and permissions information is available at www.nature.com/reprints.

Correspondence and requests for materials should be addressed to M.M.

Publisher's note: Springer Nature remains neutral with regard to jurisdictional claims in published maps and institutional affiliations.

Methods

Digestion of silica. Dissolution kinetics of several forms of BSi and LSi were compared using different digesters. As BSi, we used nitric-acid-cleaned frustules of *T. weissflogii* (cultured using F2 media), needle-like (oxea) spicules of *P. ficiformis* and star-like spicules (cortical spherasters) of *C. caribensis*. As LSi, we used aluminosilicate bentonite (Sigma-Aldrich, Pcode 101190698, $H_2Al_2O_6Si$) and kaolinite (Fluka, Pcode 100981947, $Al_2O_3{\cdot}2SiO_2{\cdot}2H_2O$). Varying dry weights for the different materials were used in the digestions (Supplementary Table 1), so that the total amount of Si to be released during the digestion was similar across the materials (1.25 ± 0.09 mgSi). To make sure that the resulting DSi concentrations always remained far below the saturating concentration, we increased the volume of digester from 10 ml (traditional approach) to 40 ml, which provided solvent in great excess. All the digestions were based on eight replicated subsamples of each material. The assayed digestion solutions were sodium carbonate at 1% (ref. [5]), 5% (ref. [21]) and 22% (ref. [23]), as well as sodium hydroxide at 0.2 M (ref. [25]) and 0.5 M (ref. [26]).

Digestions were conducted in 50 ml hermetically closed Teflon bombs immersed in distilled water at 85 °C with orbital agitation, using a 50 l SBS TBA-30 bath that was user modified for agitation and temperature control. Sodium carbonate digestions at 1, 5 and 22% were sampled at 0, 2, 3, 4, 5, 6, 8, 12, 24, 48, 60, 72 and 84 h. The more aggressive sodium hydroxide digestions (0.2 and 0.5 M) were sampled at 0, 0.75, 1.5, 2.25, 3, 4, 5, 6, 8, 12, 24, and 28 h. For each sample, 1 ml of the digestion solution was pipetted out after centrifugation of the Teflon bombs at 1,500 rpm for 3 min. The sampled digestion solution was added to 19 ml of HCl solution for buffering and termination of the digestion reaction, with the pH of the resulting mix brought down to 6, an optimal value for the colorimetric determination of Si concentration (±1%) using an Alliance Futura autoanalyser. Finally, the percentage of Si released during the digestions was plotted against time to depict between-material differences in the dissolution kinetics. Additionally, two spare Teflon tubes of each material were poured on a 0.45 cm polycarbonate filter (3 µm pore) at each sampling time. The retained particulate BSi material was subsequently inspected under a Hitachi TM3000 SEM equipped with an energy dispersive X-ray spectrometer for microanalysis, and subsequently carbon coated and examined under a high-resolution Jeol Field Emission J1700S SEM.

To digest sediment from the cores, we used sodium carbonate at 1%, following DeMaster's technique[27,48]. The method assumes that most of the BSi is dissolved in about 3 h at 85 °C and that the additional Si leached from the LSi can be corrected using the intercept of the linear regression to depict the increase in DSi caused by the progressive LSi digestion during 3, 4 and 5 h. Analyses were based on five sediment subsamples of 30 mg each.

Sediment cores. The investigated cores (Supplementary Table 2) represent a diverse array of sedimentary marine environments (Supplementary Information (Discussion 1)). Cores 1 (Challenger, Dec-58, 51719_13; Porcupine Seabigth, Northeastern Atlantic), 12 (James Cook 120–081, GC-05; Northeastern Pacific basin), 14 (Sonne SO200, SO200/15PC; Sumatra margin, Indian Ocean) and 16 (James Clark Ross, JR179, PC501; Southern Ocean) were provided by the British Ocean Sediment Core Research Facility (of the National Oceanography Centre. Cores 2 (Hudson 20110310062-pc; Flemish Cap plateau, Northwestern Atlantic) and 4 (2009061 0058 A; Flemish Cap seamount, Northwestern Atlantic) were provided by the Geological Survey of Canada, Marine Geoscience Collection Facility at the Bedford Institute of Oceanography. Core 3 (SRQ3-KS34; Bay of Brest, Northeastern Atlantic) was supplied by the Marine Geoscience research unit at IFREMER. Core 5 (MLB2017-001-006; Sambro Bank, Northwestern Atlantic) was a push core sampled in September 2017 by using ROPOS ROV on the Nova Scotia shelf during the SponGES H2020 project. Cores 6 (K11-ERGAP2; Galicia Bank, Northeastern Atlantic), 8 (TG 36, GC-88-1; Mediterranean Iberian margin), 9 (KF14, VALSIS; Valencia Trough, Western Mediterranean), 10 (TG51bis, GC86-2; Gulf of Cadiz, Northeastern Atlantic), 11 (ALM6, MAYC-96; Alboran Basin, Western Mediterranean), 13 (TG3, ORINOCO97; Guiana Basin adjacent to Demerara Plain, Northwestern Atlantic) and 17 (TG15, MAGIA-99; Bransfield Strait, Antarctic Peninsula, Antarctica) were provided by the Marine Geosciences department at the Institute of Marine Sciences (ICM, CSIC). Core 7 (C-2000; Mediterranean Iberian Margin) was provided by the Macrophyte Ecology Group at the Center for Advanced Studies of Blanes (CEAB, CSIC). Core 15 (NEA 3, 1987, 75/GC05; Great Barrier Reef, Queensland Trough) was provided by Australian Geosciences. Coring was based on gravity (cores 1, 3, 8, 10, 11, 12, 13, 15 and 17), piston (cores 2, 6, 7, 9, 14 and 16), box-core (core 4) or push-core (core 5) methodologies. All the sediments were dried to a constant weight before digestion and microscopy analyses.

Determination of dark BSi. For the microscope determination of sponge, radiolarian and silicoflagellate BSi in sediments (mgSi per gram of dry sediment), three dry sediment subsamples of 10 mg each were collected and transferred to test tubes, boiled in HCl to remove calcareous skeletons, then in nitric acid to digest organic matter, rinsed in distilled water and 100% ethanol, and sonicated for 15 min to minimize the sediment aggregates. Sediment was then pipetted out and dropped on a microscope glass slide to make sets of 10–100 smear slides per sample, depending on the sediment features. Once all the particulate material in each test tube was recovered on the slides, examination was conducted by four different observers through contrast-phase compound microscopes. Using digital cameras and morphometric software, the volumes of the different skeletal pieces were calculated, often decomposing the global structure into smaller subparts more easily assimilable to cylinders, cones, spheres or other familiar volumetric figures. Measured BSi volumes were subsequently converted into Si biomass through average density values of 2.12 g cm^{-3} for marine sponges[49], 2.0 g cm^{-3} for silicoflagellates[50] and 1.9 g cm^{-3} for radiolarians[51] (Supplementary Methods). Dried, uncoated sediment samples were also inspected randomly under a FSI Quanta 200 SEM equipped with a Genesis EDAX-EBS microanalyser to investigate the aspect and level of digestion of buried spicules.

The contribution of diatoms was indirectly estimated from the total BSi content yielded by the 1% sodium carbonate method after discounting the contribution due to dissolution of sponge spicules (16.2%), a percentage experimentally determined after 5 h of digestion of the spicules in 1% sodium carbonate (Fig. 1a). This led to a non-conservative estimate of diatom contribution, which incorporated both: (1) the BSi contribution by radiolarians (assumed to be negligible) and (2) that by the many tiny silica fragments no longer recognizable as sponge spicules in microscopy examinations.

Preservation and burial of dark BSi. The sediment deposition rates and age for each core were obtained or calculated from geological studies, as referenced in Supplementary Information (Discussion 1). The preservation during burial of sponge and radiolarian BSi was calculated from the difference (%) in the amount of BSi microscopically determined at the sediment surface and a burial depth of 50 cm (but 23 cm for push core 5). This threshold in burial depth was selected because it ensures saturation of the interstitial water with silicate[8,11,21,38], so that the seawater no longer has the chemical capability to dissolve BSi substantially. Therefore, it can be assumed that BSi preservation and diagenesis start at that threshold depth irrespective of sediment features, with BSi (that is, opal A) progressively becoming opal CT, and eventually chert[51]. For the calculations, it was also assumed that there was a constant rate of sponge BSi deposition in each core during the time required to build the involved sediment thickness (Supplementary Information (Discussion 3)). The mean rate of sponge BSi burial per year was calculated from the values of the sediment density and the mean mass of sediment deposition per metre squared and year that would be needed to build 50 cm of sediment in the number of years indicated by the age of the sediment at 50 cm. To estimate the global burial fluxes, the extension of the relevant ocean compartments for sponges and radiolarians was accurately calculated using ArcGis Software on a digital mapping of ocean bottom morphology[41]. The layer of continents was based on the Shuttle Radar Topography Mapping (SRTM30_PLUS, NGA, NASA). The layers that contain ocean geomorphology features were downloaded from www.bluehabitats.org[41], except for coral reefs, which was obtained from World Resource Institute (www.wri.org). As the map and geomorphological layers were all in the WGS84 geographical coordinates system, areas cannot be calculated directly from ArcGIS unless converted into a system of projected coordinates. There are between-projection differences in area calculation, depending on the particular algorithm for the projection (cartographic, cylindrical, pseudo-conical and so on). Therefore, to minimize errors in area determinations, we used three different projection systems (Sinusoidal or Mercator, Cylindrical Equal Areas and Bone), all of which preserve the area and reduce the projection distortion. After averaging the three projections, the areas were finally calculated using the Interset module of ArcGis. As a test, we corroborated that the total ocean area calculated by our method deviates only −0.09% from the most recent published calculation[41]. The extension of radiolarian-rich sediments was calculated using ArcGis Software from the layers available at www.earthbyte.org/webdav/ftp/papers/Dutkiewicz_etal_seafloor_lithology/, originally provided by Dutkiewicz et al.[36].

Spicules in the sediment of the cores were carbon coated and studied under a high-resolution Jeol Field Emission J1700S SEM to examine in detail the marks and progress of BSi dissolution at 0 and 50 cm burial depths.

Data availability

The authors declare that all other data supporting the findings of this study are available within the article and its Supplementary Information. Further additional data are available at the institutional repository of the Spanish National Research Council (CSIC), http://hdl.handle.net/10261/184130.

The map layers that contain the ocean geomorphology features were downloaded from www.bluehabitats.com, except for coral reefs, which were obtained from the World Resource Institute (www.wri.org). The extension of radiolarian-rich sediments was calculated using the map layers available at the www.earthbyte.org/webdav/ftp/papers/Dutkiewicz_etal_seafloor_lithology/.

References

48. DeMaster D. J. in *Marine Particles: Analysis and Characterization* (eds Hurd, D. C. & Spenser, D. W.) 363–367 (Geophysical Monographs Vol. 63, American Geophysical Union, 1991).
49. Sandford, F. Physical and chemical analysis of the siliceous skeletons in six sponges of two groups (Demospongiae and Hexactinellida). *Microsc. Res. Tech.* **62**, 336–355 (2003).
50. Hurd D. C. in *Silicon Geochemistry and Biochemistry* (ed. Aston, S. R.) 187–244 (Academic, 1983).
51. DeMaster D. J. in *Sediments, Diagenesis, and Sedimentary Rocks* (ed. Mackenzie, F. T.) 97–98 (Treatise on Geochemistry, Vol. 7, Elsevier, 2003).

nature geoscience

SUPPLEMENTARY INFORMATION

https://doi.org/10.1038/s41561-019-0430-7

In the format provided by the authors and unedited.

Sponge skeletons as an important sink of silicon in the global oceans

Manuel Maldonado[1]*, María López-Acosta[1], Cèlia Sitjà[1], Marta García-Puig[1], Cristina Galobart[1], Gemma Ercilla[2] and Aude Leynaert[3]

[1]Center for Advanced Studies of Blanes (CEAB), Spanish National Research Council (CSIC), Girona, Spain. [2]Institute of Marine Sciences (ICM-CSIC), Barcelona, Spain. [3]University of Brest, CNRS, LEMAR, Plouzané, France. *e-mail: maldonado@ceab.csic.es

SUPPLEMENTARY INFORMATION

Sponge skeletons as an important silicon sink in the global oceans

Manuel Maldonado[1]*, María López-Acosta[1], Cèlia Sitjà[1], Marta García-Puig[1], Cristina Galobart[1], Gemma Ercilla[2], Aude Leynaert[3]

[1]Center for Advanced Studies of Blanes (CEAB). Spanish National Research Council (CSIC), Acceso Cala St. Francesc 14, Blanes, 17300, Girona, Spain.
[2]Institute of Marine Sciences (ICM-CSIC). Passeig Marítim de la Barceloneta, 37-39, Barcelona 08003, Spain.
[3]University of Brest, CNRS, LEMAR, F-29280, Plouzané, France

* Corresponding author: maldonado@ceab.csic.es

Supplementary Table 1. Summary of mean (±SD) weight (mg) of siliceous material (W) initially added to be digested in the various digesters, along with the weight (mg) of silicon (Si) contained in each material sample. Eight replicates of each material were digested in each experiment.

MATERIAL		Sodium carbonate			Sodium hidroxide	
		1%	5%	22%	0.2M	0.5M
Frustules of *Thalassiosira*	W	2.50 ± 0.00	2.50 ± 0.00	2.50 ± 0.00	2.50 ± 0.01	2.50 ± 0.01
	Si	1.12 ± 0.00	1.25 ± 0.00	1.19 ± 0.00	1.03 ± 0.01	1.08 ± 0.00
Spicules of *Petrosia*	W	3.00 ± 0.01	3.00 ± 0.01	3.00 ± 0.01	3.00 ± 0.01	3.00 ± 0.00
	Si	1.37 ± 0.00	1.40 ± 0.00	1.46 ± 0.00	1.24 ± 0.00	1.34 ± 0.00
Spicules of *Chondrilla*	W	3.33 ± 0.01	3.33 ± 0.01	3.33 ± 0.00	3.33 ± 0.00	3.33 ± 0.01
	Si	1.27 ± 0.00	1.35 ± 0.00	1.27 ± 0.00	1.16 ± 0.00	1.16 ± 0.00
Bentonite	W	8.98 ± 0.01	8.99 ± 0.01	8.98 ± 0.01	8.98 ± 0.01	8.98 ± 0.00
	Si	1.26 ± 0.00	1.26 ± 0.00	1.26 ± 0.00	1.26 ± 0.00	1.26 ± 0.00
Kaolinite	W	6.44 ± 0.01	6.44 ± 0.01	6.43 ± 0.01	6.44 ± 0.01	6.44 ± 0.01
	Si	1.26 ± 0.00	1.26 ± 0.00	1.26 ± 0.00	1.26 ± 0.00	1.26 ± 0.00

Supplementary Table 2. Summary of core features, including original cruise labels, geomorphological and geographical settings, coordinates, and depth. Core numbers were given according to North-to-South latitude of the collection site. See Supplementary Discussion 1 for further details and references.

Core #	Core label	Ocean or sea	Seafloor compartment	Geographical site	Latitude (º)	Longitude (º)	Depth (m)
1	51719_13	NE Atlantic	Slope basin	Porcupine Seabigth	51.058	-12.912	2025
2	FC062	NW Atlantic	Seamount	Flemish Cap	48.7728	-45.46625	1163
3	KS34	NE Atlantic	Continental shelf	Bay of Brest	48.3133	-4.40945	15.5
4	0058A	NW Atlantic	Seamount	Geodia ground, Flemish cap	46.8487	-43.750446	830
5	MLB2017	NW Atlantic	Continental shelf	Vazella ground, Sambro Bank	43.89	-63.076	160
6	K11	NE Atlantic	Seamount	Galicia Bank	42.8848	-11.56047	2119
7	C2000	Mediterranean	Continental shelf	Portlligat	42.2917	3.29001	3
8	TG36	Mediterranean	Continental rise	Girona	42.017	3.902	1900
9	KF14	Mediterranean	Basin	Balearic Sea	40.527	3.50166	2070
10	TG51bis	NE Atlantic	Continental shelf	Gulf of Cadiz	36.7818	-6.96633	124
11	ALM6	Mediterranean	Basin	Alboran Sea	36.3562	-2.61866	1456
12	JC120	NE Pacific	Abbysal plain	Equatorial Northeastern Pacific	16.9132	-122.99695	4290
13	TG3	NW Atlantic	Continental rise	Adjacent to Demerara Plain	11.1964	-54.36472	4739
14	SO200	Indian Ocean	Continental slope	Sumatra	-0.8594	97.81493	3840
15	75/GC05	SW Pacific	Continental slope	Great Barrier Reef	-16.42	146.21	1100
16	PC501	SE Pacific	Abbysal plain	Southern Ocean	-60.5347	-108.3028	5204
17	TG15	SW Atlantic	Continental slope	Antarctic Peninsula	-62.9319	-59.4631	882

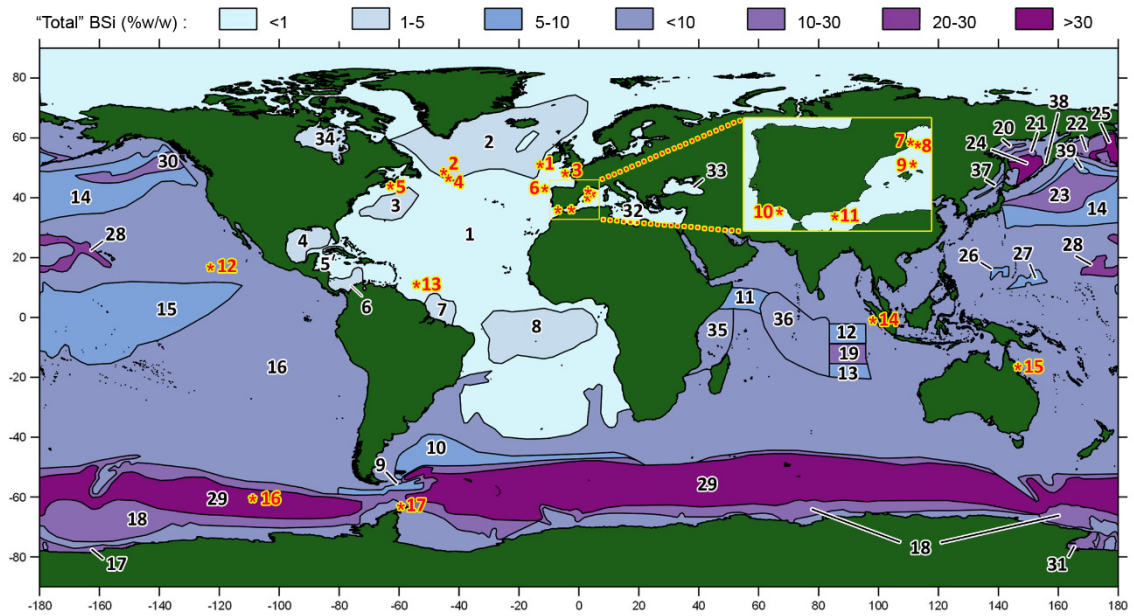

Supplementary Fig. 1 | Geographical location of examined sediment cores relative to the distribution of "total" BSi at the seafloor (updated after Lisitzin[1,2], Hurd[3], and Dittert[4]). Sampled sediments (yellow asterisks and numbers) represent a wide variety of marine environments. Cores were numbered in increasing order according to the latitude of the collection site, from North to South. Further information on cores can be found in Supplementary Table 1 and in Supplementary Discussion 1. Pioneering work by Lisitzin summarized the gross distribution of "total" BSi (as weight % of dry sediment) in the uppermost sediment layer of the world's oceans. He did it so by digesting 2000 sediment samples in hot 5% sodium carbonate for 5 hours, a method herein demonstrated to dissolve only 53.76 ± 1.98% and 48.81±2.45% of the spicules mass of *Petrosia ficiformis* and *Chondrilla caribensis*, respectively. Therefore, it underestimated about 50% of the sponge BSi in the sediments. Despite that shortcoming, the gigantic Lisitzin's work became of widespread importance. It established the notion of 3 "belts" of recent BSi accumulation, grossly reflecting global patterns of abundance of diatoms and radiolarians in the water column: 1) an almost continuous, 1000 to 2000 km-wide band around the globe in the Southern Ocean, with a northern limit at the Antarctic Convergence (45ºS to 55ºS); 2) an equivalent similar northern band, better developed in the Pacific, Japan Sea and Bering Sea; and 3) a nearly-equatorial 20ºN-20ºS band in the Indian and Pacific Oceans, which is less marked in the Atlantic Ocean. Lisitzin's mapping also established the notion that siliceous sediments are poorly represented between the parallels 20º and 40º in northern and southern hemispheres, roughly coincidentally with zones of low abundance of diatoms and radiolarians in the plankton[2]. Those general patterns fostered the view that the BSi accumulating at the ocean bottom proceeded almost exclusively from a rain of siliceous planktonic organisms, which indirectly led to consider as irrelevant any further attempt to estimate the BSi contribution from benthic organisms. Despite the significance of Lisitzin's work, the truth is that the method he used to digest sediments missed not only about half of the sponge BSi, but, as noticed by DeMaster[5], it also dissolved an undetermined amount of lithogenic silica, for which no correction was ever applied. Here we have shown (Fig. 1) that his method dissolves aluminum-silicate benthonite and kaolinite in about 11.95 ± 0.34 % and 3.08 ± 0.12 %, respectively.

Supplementary Discussion 1. The investigated cores stand for a wide array of depositional environments. Continental shelves are represented by core 3 (Bay of Brest, France, North Eastern Atlantic)[6], core 5 (Sambro Bank, Canada, North Western Atlantic)[7,8], core 7 (Portlligat Bay, Spain, Western Mediterranean)[9,10], and core 10 (Gulf of Cadiz, Spain, North Eastern Atlantic)[11]. All 5 cores account for markedly different depositional environments. For instance, cores 3 and 7 come from shallow bays, but the former with high primary productivity and a detrital bottom hosting a rich sponge community[12], while the latter has oligotrophic conditions and a sandy bottom almost entirely occupied by a sea grass meadow and a comparatively poor sponge fauna. Yet this

latter bay appears to function as a concentration area that accumulates resuspended materials from adjacent shelf bottoms, what would explain the abundance of sponge spicules, including skeletal pieces from species that are not known to live within the bay. Cores 5 and 10 come from the distal zone of the continental shelf, and, more importantly, core 5 accounts for a dense monospecific aggregation of the hexactinellid sponge *Vazella pourtalesii*[13], while core 10 comes from a deltaic area with sediments at the distalmost continental shelf, where sponges are rare.

Continental slopes are represented by cores 14 (Sumatra margin, Eastern Indian Ocean), 15 (North Eastern Australian, Great Barrier Reef Slope, Western Pacific), and 17 (Antarctic slope, Southern Ocean). Cores 14 and 15 are from sediments receiving deposition from coral reef assemblages above[14,15]. Core 17 received deposition from rich siliceous benthic and planktonic communities in the area of the Bransfield Strait (Antarctica)[16,17,18].

Seamounts and plateaus are represented by cores 2, 4, and 6. The latter core receives deposition from the sponge-rich benthic community at the Galicia Bank seamount (Northeastern Atlantic)[19,20,21]. Cores 2 and 4 come from the slope of Flemish Cap Plateau (Northwestern Atlantic, off Canada)[22,23,24], but core 4 was sampled from an aggregation of *Geodia* spp. sponges, while core 2 is from an area with scarce sponge presence. It is also worth noting the peculiarity of the Recent depositional environment in core 2, with Holocene sedimentation rates (0.01-0.02 mm y^{-1}) being sufficiently low and bottom current strength sufficiently high to erode away modern sediments, minimizing rates of BSi accumulation in the upper sediments and burial. The layer of exposed sediment at the bottom, according to correlations with Heinrich Layer stratigraphy[25], appears to be about 12 ky old, therefore reflecting a combination of Pleistocene preservation and Holocene deposition.

The continental rise is represented by cores 8 and 13. The former receives deposition from productive pelagic communities of the Gulf of Lion (Northwestern Mediterranean), influenced by the terrestrial inputs of seasonal Girona rivers[26] and Rhône River[27,28]. Core 13 (Subequatorial Southwestern Atlantic) receives the depositional influence from the Orinoco River mouth[29,30] and is adjacent to Demerara Abyssal Plain. Because their open-water nature, those sediments were included in the "basin" compartment. Both areas are poor in sponge fauna.

The basin bottoms are represented by cores 1, 9, 11, 12, and 16, but, again, with important between-core differences in depositional environments. Core 1 (Southwest of

Ireland, Northeastern Atlantic)[31], located in the northern zone of the slope basin "Porcupine Seabight", might receive depositions from local sponge aggregations[32,33]. Cores 9[34] and 11[35,36] are both receiving deposition from Mediterranean oligotrophic areas and comparatively sponge-poor benthic communities. Yet core 9 (northern Balearic Sea)[37] represents even a less productive Mediterranean zone than core 11 (Alboran Sea)[38], since the latter might occasionally receive material from benthic assemblages on adjacent banks[39]. Core 12 (Subequatorial Northeastern Pacific)[40] receives deposition from both pelagic communities fostered by rich-nutrient upwellings and abyssal benthic communities from the adjacent Clipperton-Clarion Fracture Zone (CCFZ) [41], although with scarce sponges. Core 16 (Southern Ocean) receives deposition from rich planktonic communities commonly dominated by siliceous microorganisms and builds a benthic environment that facilitates BSi preservation[42,43,44], leading to formation of biosiliceous oozes.

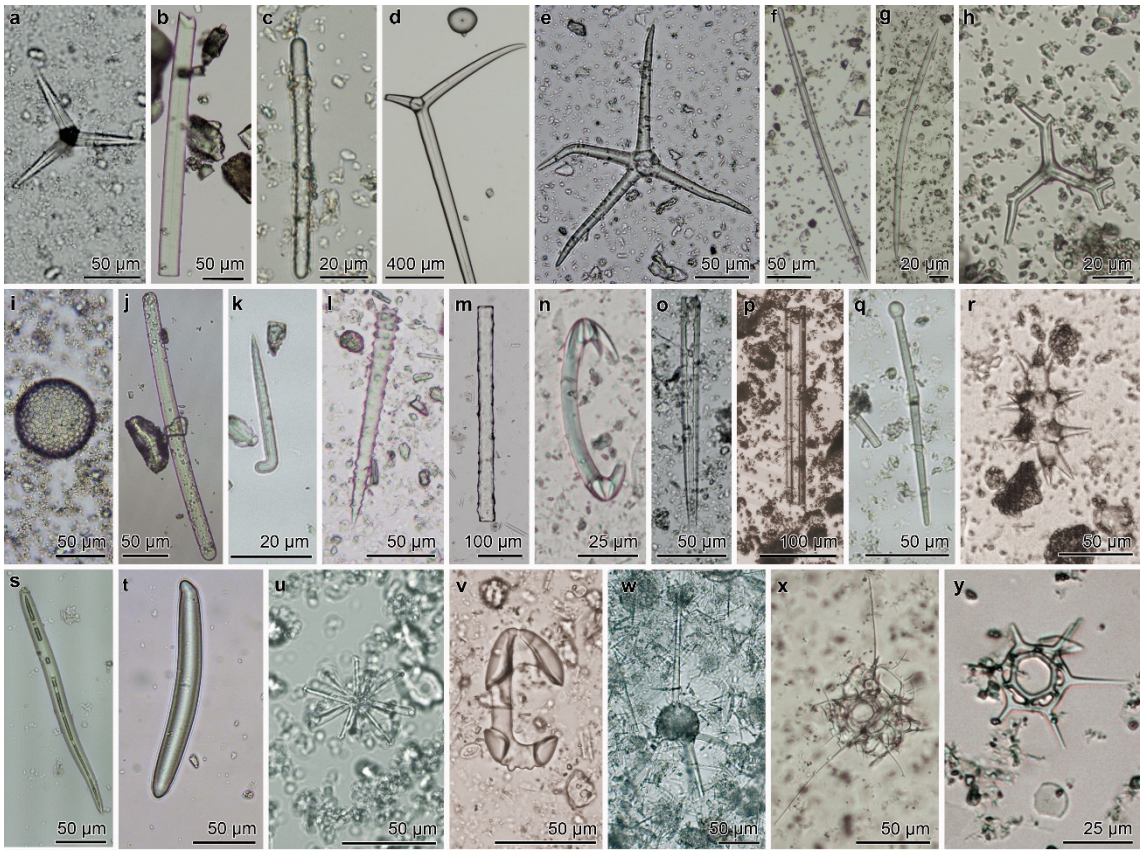

Supplementary Fig. 2 | Sponge, radiolarian and silicoflagellate BSi in sediments. a-n, Sponge spicules in the superficial sediment of core #1 (a), #2 (b), #3 (c), #4 (d), #5 (e), #8 (f), #9 (g), #11 (h), #12 (i), #13 (j), #14 (k), #15 (l), #16 (m), and #17 (n). **o-v,** Sponge spicules buried at 50 cm in core #1 (o), #2 (p), #3 (q), #6 (r), #10 (s), #13 (t), #14 (u), and #15 (v). **w-x,** Radiolarian skeletons in the superficial sediment of core 16 (w) and buried at 50 cm in core 17 (x). **(y)** Silicoflagellate skeleton buried at 50 cm in core 17. Note that delicate tiny spicules of demosponges (**r, v**) and hexactinellid (**u**) sponges are well preserved even after being buried for 14.7, 3.6 and 1.6 kiloyears, respectively.

Supplementary Table 3. Contribution (average ± SD) of diatoms, sponges, radiolarians and silicoflagellates to the BSi content in the 1-cm thick uppermost layer of sediments.

core #	BSi in uppermost sed. (mg Si g^{-1} sed.)			
	diatoms	sponges	radiolaria	silicoflagellates
	avg ± SD	avg ± SD	avg ± SD	avg ± SD
1	1.875 ± 0.436	0.080 ± 0.034	0.148 ± 0.005	0 ± 0
2	2.383 ± 0.514	1.275 ± 0.284	0.242 ± 0.132	0 ± 0
3	1.472 ± 0.169	1.391 ± 0.241	0 ± 0	0 ± 0
4	0.142 ± 0.310	76.314 ± 38.147	0.078 ± 0.079	0 ± 0
5	0.424 ± 0.165	0.334 ± 0.026	0.001 ± 0.000	0.0004 ± 0.0001
6	0.515 ± 0.123	2.491 ± 0.297	0.042 ± 0.017	0 ± 0
7	0.022 ± 0.033	0.496 ± 0.300	0 ± 0	0 ± 0
8	1.073 ± 0.101	0.012 ± 0.007	0 ± 0	0 ± 0
9	1.033 ± 0.131	0.045 ± 0.064	0 ± 0	0 ± 0
10	1.029 ± 0.066	0.042 ± 0.023	0.0001 ± 0.0001	0 ± 0
11	0.701 ± 0.123	0.061 ± 0.034	0 ± 0	0 ± 0
12	0.715 ± 0.190	0.135 ± 0.026	0 ± 0	0 ± 0
13	1.228 ± 0.120	0.287 ± 0.069	0 ± 0	0 ± 0
14	2.471 ± 0.249	1.044 ± 0.896	0.051 ± 0.050	0 ± 0
15	0.333 ± 0.166	0.587 ± 0.042	0.015 ± 0.018	0 ± 0
16	98.564 ± 8.534	0.125 ± 0.003	5.936 ± 1.301	0.173 ± 0.044
17	45.692 ± 2.316	2.572 ± 0.861	0.026 ± 0.010	0 ± 0

Supplementary Discussion 2. The abundance of sponge BSi in sediments, herein quantified for the first time, was long suspected. For instance, several Ocean Drilling Program Reports warned literally that "the scarcity of studies on sponge spicules is not because of a lack of spicules, as spicules are often abundant in marine sediments"[45,46]. Microscopy inspection of sediments from the continental rise and abyssal plane at the Gulf of Mexico ranked spicules as "abundant" to "dominant", whereas diatoms and radiolarians were only "frequent" to "common". Sponge spicules also occurred in 96% of the 1,426 sediment samples collected from open waters deeper than 200 m in the North Atlantic[47]. Spicules have been reported to dominate BSi sediments of coral reefs[48] and rocky coasts[49]. They also form meter-thick mats at the continental shelf and slope in Arctic and Antarctic areas[50,51].

Supplementary Discussion 3. Sponges are sessile organisms. Unlike in the case of diatom frustules, their siliceous spicules do not reach the sediment as a rain from the water column, but experiencing restricted lateral transport and limited resuspension from the decaying sponge bodies. Consequently, rates of deposition and burial of sponge BSi are

little related to the sediment deposition rate (Supplementary Fig. 5), except for the fact that the faster sediment deposition, the faster the burial of sponge BSi. In general, the magnitude of sponge BSi burial is expected to be more related to both the local abundance of sponge communities[51,52,53,54] and episodic events of massive sponge mortality[55,56].

Mean rates of sponge BSi burial spanned two orders of magnitude across cores of the "continental-margin-&-seamount" compartment. It reflects the large variety of depositional environments that were sampled. It also means that the approach is considering both the very positive and negative environments in terms of sponge BSi abundance and burial (i.e., sponge aggregations vs. areas with very poor sponge fauna), along with different intermediate situations. In consequence, subsequent additions of information coming from the study of new cores is more likely to reduce the errors associated to our means than to modify substantially the mean themselves. For this reason, our approach is expected to be resilient to the addition of future data.

For calculating preservation of both sponge and radiolarian BSi, a constant rate of BSi deposition within each core for the time period required to build 50 cm of sediment is assumed. Such period ranged from 440 to 14,700 years in the set of cores, being core 12 a 74,000 years-old outlier (Table 2). There is evidence that some sponge grounds have existed continuously over the last 130 milennia[24], that glass-sponge reefs have been growing continuously through the last 9,000 years[57], and that the growth of some giant hexactinellid spicules required up to 11,000 years to be completed[58]. These examples of extreme individual and population longevity indicate that the sponge assemblages, particularly in deep waters, have relatively slow dynamics and that can be stable over periods of millennia. Relatively constant rates of BSi deposition are therefore plausible over the concerned periods.

Our approach yielded overrated (>100%) sponge BSi preservation in four cores (i.e., 23.5% of cores). Interestingly, three of those cores (#3, 16, 17) came from sites where rates of accumulation and preservation for diatom BSi are known to be greater than in the rest of the ocean[44,59]. These overrated preservations likely reflect favorable conditions for BSi preservation[44,60,61] coupled to past local episodes of massive mortality in the sponge assemblages[55]. In a fourth core (#8), sponge BSi occurred in extremely low values, the lowest in the study. Under such BSi scarcity, the finding by pure chance of one more or one less spicule in sediment replicates from 0 cm or in those from 50 cm may have an impact on the estimated average preservation (%). For these reasons, overrated cores were never considered when calculating average preservation for sponge BSi. For

subsequent calculations involving the overrated cores, the average BSi preservation (45.2±27.4%) resulting from the 13 remaining cores was used. This made a conservative approach, since an averaged preservation is used for sediments in which preservation is known to be greater[44,59,62] than the average in marine sediments. Interestingly, the resulting average for sponge BSi preservation comes into general agreement with an approximate 50% decrease in the number of sponge spicules between 0 and 50 cm noticed in the only available studies of coastal sediments in this regard[49,63].

In the case of radiolarians, preservation was also overrated in the same two cores of the Southern Ocean (#16, 17) than sponge BSi did, and, again, in core 10, where radiolarians recorded their lowest abundance. As for sponges, the three overrated cores were never considered when calculating average preservation of radiolarian BSi. Any calculation involving the overrated cores was based on the average preservation value (6.8%) resulting from the rest of cores. In this regard, a scenario considering a radiolarian BSi preservation of only 6.8% in the biosioliceous oozes (scenario 1 in Supplementary Table 4) can be defined as very conservative. Therefore, we explored two plausible alternative scenarios to evaluate the effect of such constraint. An alternative scenario (scenario 2) was to assume that the preservation of radiolarian BSi in the biosiliceous oozes would be similar to the average preservation (10.2%) estimated for BSi in sediments of the Southern Ocean[62]. Under this scenario, a global burial flux of 11.3±5.0 x 10^{-2} Tmol Si y^{-1} resulted for radiolarians. A third scenario (scenario 3) was to assume a radiolarian preservation in the oozes equal to the maximum preservation found in our set of cores (28.7%). It yielded a global burial flux of 20.4±5.6 x 10^{-2} Tmol Si y^{-1}. Altogether, it means that, even when using relaxed scenarios for BSi preservation, the global burial flux of Si through radiolarian skeletons consistently results in a modest contribution, ranging from 0.09 to 0.20 Tmol Si y^{-1} (Supplementary Table 4). The mean point of that interval (0.15 Tmol Si y^{-1}) would still represent only 2.4% of the global biological sink.

Supplementary Table 4. Mean (±SD) preservation rates and burial fluxes of radiolarian BSi under 3 different scenarios of preservation (%) in the biosiliceous oozes. Scenario 1 assumes preservation of 6.8%, as resulting from the average of the investigated cores, Scenario 3 assumes the maximum preservation found in our set of cores (28.7%). Scenario 2 considers an intermediate preservation (10.7%), which corresponds to the value estimated in the literature[62] for BSi preservation in the Southern Ocean.

OCEAN COMPARTMENT	Compartment extension (km^2 x 10^6)	Radiolarian BSi preservation (mg Si m^{-2} y^{-1})			Radiolarian BSi burial flux (Tmol Si y^{-1})		
		Scenario 1 6.8%	Scenario 2 10.7%	Sceneario 3 28.7%	Scenario 1 6.8%	Scenario 2 10.7%	Scenario 3 28.7%
radiolarian oozes	5.340	38.74 ± 8.49	61.17 ± 13.41	163.91 ± 35.92	0.01 ± 0.00	0.01 ± 0.00	0.03 ± 0.01
radiolaria-rich diatom oozes	19.464	38.74 ± 8.49	61.17 ± 13.41	163.91 ± 35.92	0.03 ± 0.01	0.04 ± 0.01	0.11 ± 0.02
rest of "radiolarian" ocean	337.076	4.91 ± 11.98	4.91 ± 11.98	4.91 ± 11.98	0.06 ± 0.10	0.06 ± 0.10	0.06 ± 0.10
GLOBAL OCEAN	361.880	--	--	--	0.09 ± 0.05	0.11 ± 0.05	0.20 ± 0.06

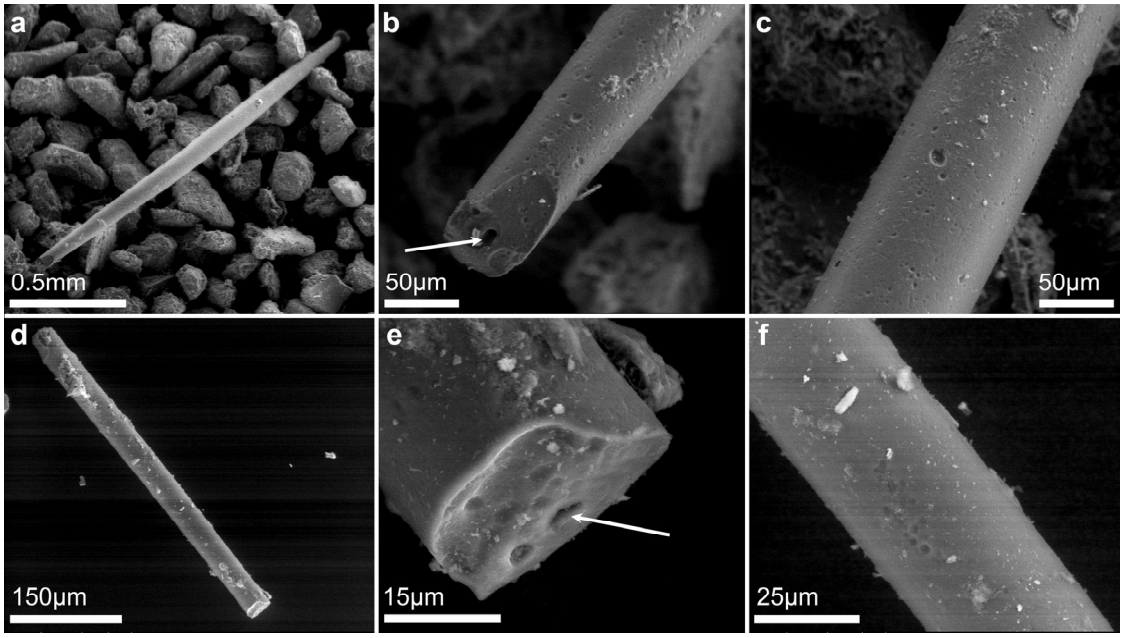

Supplementary Fig. 3 | Buried sponge spicules. a-c, Nearly entire tilostyle buried in 5m of highly carbonated, 4,500 year-old sediments of a *Posidonia oceanica* meadow (core 7). Despite this sediment favoring BSi digestion, both the axial canal (**b**, arrow**)** and the spicule surface (**c**) show only incipient signs of dissolution, revealed by tiny pits. **d-f,** Spicule fragment (**d**) in the same sediment sample, showing an axial canal (**e**, arrow) that has not yet been widened by dissolution. Likewise, the spicule surface shows only incipient signs of dissolution in the form of small pits (**f**).

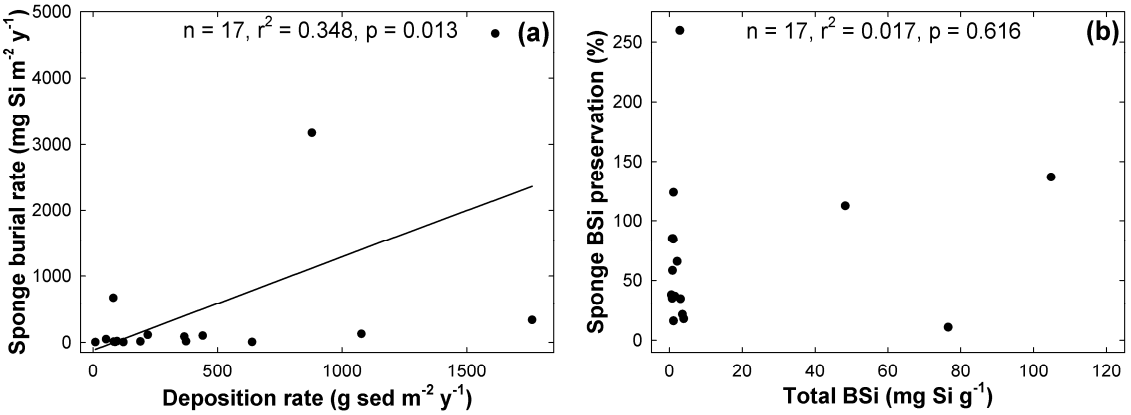

Supplementary Fig. 4 | a, The burial rate of sponge BSi poorly correlates the rate of sediment deposition, in agreement with a previous study[49]. This is so because sponges are sessile and, unlike in the case of planktonic diatoms, their BSi does not reach the sediment as a silica rain from the water column, but rather through restricted lateral transport and limited resuspension from the decaying bodies. The magnitude of the sponge BSi burial will depend primarily on the local abundance of sponges. The sediment deposition rate will mostly determine the speed at which the sponge BSi gets buried, minimally affecting the magnitude of the sponge BSi burial flux. **b,** Sponge BSi preservation (%) does not correlate total BSi in the sediments. This is apparently shocking, since chemical rules dictate that the level of total BSi in sediments controls the DSi saturation of the interstitial seawater and, therefore, its avidity to dissolve BSi structures, a process well known from diatom frustules. Yet, there is also experimental evidence that sponge BSi is refractory to dissolution in DSi-unsaturated seawater[52] and basic solutions[64, this study], what disrupts the theoretically expected relationship. The reasons for the comparatively high resistance to dissolution of the sponge BSi remain unclear, but its complexation with dissolution-resistant organic molecules such chitin[65] could be involved.

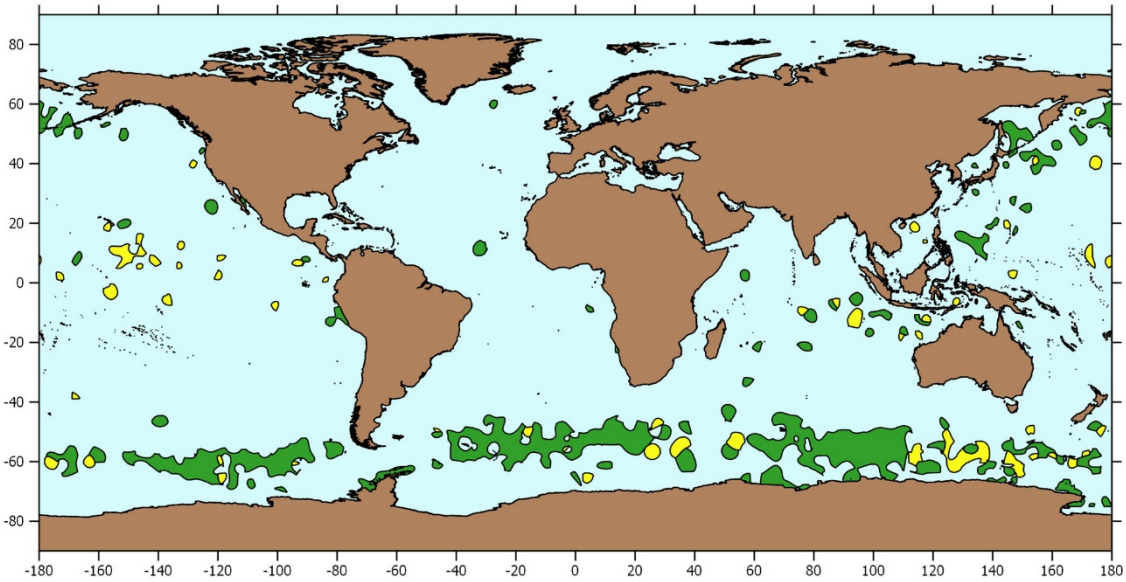

Supplementary Fig. 5 | Radiolarian-rich ooze. Patches of ocean floor where sediments contain abundant skeletons of siliceous radiolarians. Radiolarian oozes are in yellow and radiolarian-rich diatom oozes are in green (modified from Dutkiewicz *et al*[61]; see Methods).

Supplementary Methods. Sediment age was calculated from deposition ratios or age information available in the scientific literature of either the cores themselves or sediments from adjacent sites, as it follows: core 1[31] core 2[24], core 3[66], core 4[23], core 5[7,8], core 6[20,21] , core 7[10], core 8[27,67], core 9[34,37], core 10[11], core 11[35,36], core 12[40], core 13[29,30], core 14[68], core 15[15], core 16[42], core 17[16,17,18]. Sediment biomass was obtained from the wet bulk density, either obtained from the above-cited literature or estimated from core depth through the Tenzer and Gladkikh's regression equation[69],

$$\rho\,(D) = [1.66 \pm 0.02] - D \times [(5.1 \pm 0.5) \times 10^{-5}],$$

where "ρ" is density in g cm^{-3}, "D" is ocean depth in m, "1.66" is the nominal sediment density of the upper sedimentary layer at sea level, and "5.1 x 10^{-5}" is a coefficient reflecting that density decreases proportionally (relative to the nominal value) at a rate of -0.051 g cm^{-3}.

Density values of BSi vary across organism types. For sponges, it varies from 2.03 to 2.13 g cm^{-3}, depending on the species[70]. Density varies from 1.7 to 2.1 g cm^{-3} in radiolarian silica[71]. In the calculations, we have used values of 2.12 g cm^{-3} for marine sponges, 1.9 g cm^{-3} for radiolarians and 2.0 g cm^{-3} for silicoflagellates[72].

References

1. Lisitzin AP. *Sedimentation in the world ocean*, vol. 17. Society of Economic Paleontologists and Mineralogists: Tulsa, 1972.
2. Lisitzin AP. Distribution of siliceous microfossils in suspension and in bottom sediments. In: Funnelll BM, Riedel WR (eds). *The micropaleontology of oceans*. Cambridge University Press: Cambridge, 1971, pp 173-195.
3. Hurd DC. Interactions of biogenic opal, sediment and seawater in the Central Equatorial Pacific. *Geochim Cosmochim Acta* 1973, **37**(10)**:** 2257-2282.
4. Dittert N, Corrin L, Diepenbroek M, Grobe H, Heinze C, Ragueneau O. Management of (pale-)oceanographic data sets using the PANGAEA information system: the SINOPS example. *Computers & Geosciences* 2002, **28**(7)**:** 789-798.
5. DeMaster DJ. Measuring biogenic silica in marine sediments and suspended matter. In: Hurd DC, Spenser DW (eds). *Marine particles: Analysis and characterization*, vol. Gepohysical Monographs 63. American Geophysical Union: Washington, 1991, pp 363-367.
6. Gregoire G, Le Roy P, Ehrhold A, Jouet G, Garlan T. Control factors of Holocene sedimentary infilling in a semi-closed tidal estuarine-like system: the bay of Brest (France). *Mar Geol* 2017, **385:** 84-100.
7. Keigwin LD, Sachs JP, Rosenthal Y. A 1600-year history of the Labrador Current off Nova Scotia. *Climate Dynamics* 2003, **21**(1)**:** 53-62.
8. Piper DJW. Seabed geology of the Canadian eastern continental shelf. *Cont Shelf Res* 1991, **11**(8-10)**:** 1013-1035.
9. Mateo MA, Renom P, Michener RH. Long-term stability in the production of a NW Mediterranean *Posidonia oceanica* (L.) Delile meadow. *Palaeogeography, Palaeoclimatology, Palaeoecology* 2010, **291:** 286-296.
10. Serrano O, Mateo MA, Renom P, Julià R. Characterization of soils beneath a Posidonia oceanica meadow. *Geoderma* 2012, **185–186:** 26-36.
11. Nelson CH, Baraza J, Maldonado A, Rodero J, Escutia C, Barber JH. Influence of the Atlantic inflow and Mediterranean outflow currents on Late Quaternary sedimentary facies of the Gulf of Cadiz continental margin. *Mar Geol* 1999, **155**(1-2)**:** 99-129.
12. López-Acosta M, Leynaert A, Grall J, Maldonado M. Silicon consumption kinetics by marine sponges: An assessment of their role at the ecosystem level. *Limnol Oceanogr* 2018, **63**(6)**:** 2508-2522.

13. Beazley L, Wang ZL, Kenchington E, Yashayaev I, Rapp HT, Xavier JR*, et al.* Predicted distribution of the glass sponge *Vazella pourtalesi* on the Scotian Shelf and its persistence in the face of climatic variability. *Plos One* 2018, **13**(10)**:** e0205505.

14. Stevens SH, Moore GF. Deformational and sedimentary processes in trench slope basins of the western Sunda Arc, Indonesia *Mar Geol* 1985, **69**(1-2)**:** 93-112.

15. Dunbar GB, Dickens GR, Carter RM. Sediment flux across the Great Barrier Reef Shelf to the Queensland Trough over the last 300 ky. *Sediment Geol* 2000, **133**(1–2)**:** 49-92.

16. Masqué P, Isla E, Sanchez-Cabeza JA, Palanques A, Bruach JM, Puig P*, et al.* Sediment accumulation rates and carbon fluxes to bottom sediments at the Western Bransfield Strait (Antarctica). *Deep-Sea Res II* 2002, **49**(4–5)**:** 921-933.

17. Isla E, Masqué P, Palanques A, Guillén J, Puig P, Sanchez-Cabeza JA. Sedimentation of biogenic constituents during the last century in western Bransfield and Gerlache Straits, Antarctica: a relation to currents, primary production, and sea floor relief. *Mar Geol* 2004, **209**(1)**:** 265-277.

18. Willmott V, Domack EW, Canals M, Brachfeld S. A high resolution relative paleointensity record from the Gerlache-Boyd paleo-ice stream region, northern Antarctic Peninsula. *Quatern Res* 2006, **66**(1)**:** 1-11.

19. Serrano A, Gonzalez-Irusta JM, Punzon A, Garcia-Alegre A, Lourido A, Rios P*, et al.* Deep-sea benthic habitats modeling and mapping in a NE Atlantic seamount (Galicia Bank). *Deep-Sea Res I* 2017, **126:** 115-127.

20. Alonso B, Ercilla G, Casas D, Estrada F, Farrán M, García M*, et al.* Late Pleistocene and Holocene sedimentary facies on the SW Galicia Bank (Atlantic NW Iberian Peninsula). *Mar Geol* 2008, **249**(1–2)**:** 46-63.

21. Rey D, Rubio B, Mohamed K, Vilas F, Alonso B, Ercilla G*, et al.* Detrital and early diagenetic processes in Late Pleistocene and Holocene sediments from the SW Galicia Bank inferred from high-resolution enviromagnetic and geochemical records. *Mar Geol* 2008, **249**(1–2)**:** 64-92.

22. Murillo FJ, Serrano A, Kenchington E, Mora J. Epibenthic assemblages of the Tail of the Grand Bank and Flemish Cap (northwest Atlantic) in relation to environmental parameters and trawling intensity. *Deep-Sea Res I* 2016, **109:** 99-122.

23. Weitzman J, Ledger S, Stacey CD, Strathdee G, Piper DJW, Jarrett KA*, et al.* Logs of short push cores, deep-water margin of Flemish Cap and the eastern Grand Banks of Newfoundland: Geological Survey of Canada; 2014.

24. Murillo FJ, Kenchington E, Lawson JM, Li G, Piper DJW. Ancient deep-sea sponge grounds on the Flemish Cap and Grand Bank, northwest Atlantic. *Mar Biol* 2016, **163**(3)**:** 1-11.

25. Heinrich H. Origin and consequences of cyclic ice rafting in the Northeast Atlantic Ocean during the past 130,000 years. *Quatern Res* 1988, **29:** 142-152.

26. Ercilla G, Farrán M, Alonso B, Díaz JI. Pleistocene progradational growth pattern of the northern Catalonia continental shelf (northwestern Mediterranean). *Geo-Marine Letters* 1994, **14:** 264-271.

27. Beaudouin C, Dennielou B, Melki T, Guichard F, Kallel N, Berné S*, et al.* The Late-Quaternary climatic signal recorded in a deep-sea turbiditic levee (Rhône Neofan, Gulf of Lions, NW Mediterranean): palynological constraints. *Sediment Geol* 2004, **172**(1–2)**:** 85-97.

28. Auger PA, Diaz F, Ulses C, Estournel C, Neveux J, Joux F*, et al.* Functioning of the planktonic ecosystem on the Gulf of Lions shelf (NW Mediterranean) during spring and its impact on the carbon deposition: a field data and 3-D modelling combined approach. *Biogeosciences* 2011, **8**(11)**:** 3231-3261.

29. Damuth JE. Late Quaternary sedimentation in the western equatorial Atlantic. *Geol Soc Am Bull* 1977, **88:** 695-710.

30. Embley RW, Langseth MG. Sedimentation processes on the continental rise of northeastern South America. *Mar Geol* 1977, **25**(4)**:** 279-297.

31. Kenyon NH, Ivanov MK, Akhmetzhanov AM. Cold water carbonate mounds and sediment transport on the Northeast Atlantic margin: UNESCO; 1998.

32. Bett BJ, Rice AL. The influence of hexactinellid sponge spicules on the patchy distribution of macrobenthos in the Porcupine Seabight (bathyal NE Atlantic). *Ophelia* 1992, **36:** 217-226.

33. Rice AL, Thurston MH, New AL. Dense aggregations of a hexactinellid sponge, *Pheronema carpenteri*, in the Porcupine Seabight (northeast Atlantic Ocean), and possible causes. *Prog Oceanogr* 1990, **24:** 179-196.

34. Frigola J, Moreno A, Cacho I, Canals M, Sierro FJ, Flores JA*, et al.* Evidence of abrupt changes in Western Mediterranean Deep Water circulation during the last 50 kyr: A high-resolution marine record from the Balearic Sea. *Quatern Int* 2008, **181**(1)**:** 88-104.

35. Cacho I, Grimalt JO, Canals M, Sbaffi L, Shackleton NJ, Schonfeld J*, et al.* Variability of the western Mediterranean Sea surface temperature during the last

25,000 years and its connection with the Northern Hemisphere climatic changes. *Paleoceanography* 2001, **16**(1)**:** 40-52.

36. Nebout NC, Turon JL, Zahn R, Capotondi L, Londeix L, Pahnke K. Enhanced aridity and atmospheric high-pressure stability over the western Mediterranean during the North Atlantic cold events of the past 50 k.y. *Geology* 2002, **30**(10)**:** 863-866.
37. Sierro FJ, Hodell DA, Curtis JH, Flores J-A, Reguera I, Colmenero-Hidalgo E*, et al.* (Table 1) Age determination of sediment core MD99-2343. *Supplement to: Sierro, FJ et al. (2005): Impact of iceberg melting on Mediterranean thermohaline circulation during Heinrich events. Paleoceanography, 20(2), PA2019, https://doi.org/10.1029/2004PA001051*: PANGAEA; 2005.
38. Stambler N. The Mediterranean Sea - Primary Productivity. In: Goffredo S, Dubinsky Z (eds). *The Mediterranean Sea: Its history and present challenges*. Springer: Dordrecht, 2014, pp 113-121.
39. Würtz M, Rovere M. *Atlas of the Mediterranean seamounts and seamount-like structures*. IUCN: Gland, Switzerland, 2015.
40. Volz JB, Mogollon JM, Geibert W, Arbizu PM, Koschinsky A, Kasten S. Natural spatial variability of depositional conditions, biogeochemical processes and element fluxes in sediments of the eastern Clarion-Clipperton Check for Zone, Pacific Ocean. *Deep-Sea Research Part I-Oceanographic Research Papers* 2018, **140:** 159-172.
41. Vanreusel A, Hilario A, Ribeiro PA, Menot L, Arbizu PM. Threatened by mining, polymetallic nodules are required to preserve abyssal epifauna. *Sci Rep* 2016, **6:** 26808.
42. Jacot Des Combes H, Esper O, De la Rocha CL, Abelmann A, Gersonde R, Yam R*, et al.* Diatom $\delta^{13}C$, $\delta^{15}N$, and C/N since the Last Glacial Maximum in the Southern Ocean: potential impact of species composition. *Paleoceanography* 2008, **23**(4).
43. Alvain S, Moulin C, Dandonneau Y, Loisel H. Seasonal distribution and succession of dominant phytoplankton groups in the global ocean: a satellite view. *Global Biogeochem Cycles* 2008, **22**(3)**:** GB3001.
44. DeMaster DJ. The accumulation and cycling of biogenic silica in the Southern Ocean: revisiting the marine silica budget. *Deep-Sea Res II* 2002, **49**(16)**:** 3155-3167.
45. Ahlbach WJ, McCartney K. Siliceous sponge spicules from site 478: ODP; 1992.
46. McCartney K. Siliceous sponge spicules from Ocean Drilling Program Leg 114: ODP; 1990.

47. Murray J, Chumley J. The deep-sea deposits of the Atlantic Ocean. *Trans R Soc Edinb* 1924, **54:** 1-252.

48. Rützler K, Macintyre IG. Siliceous sponge spicules in coral reefs sediments. *Mar Biol* 1978, **49**(2)**:** 147-159.

49. Bavestrello G, Cattaneo-Vietti R, Cerrano C, Cerutti S, Sarà M. Contribution of sponge spicules to the composition of biogenic silica in the Ligurian Sea. *Pubbl Staz Zool Napoli Mar Ecol* 1996, **17**(1-3)**:** 41-50.

50. Barthel D, Tendal OS. Sponge spicules in abyssal and bathyal sediments of the NE Atlantic. *Deep-Sea Newsl* 1993, **20:** 15-18.

51. Gutt J, Böhmer A, Dimmler W. Antarctic sponge spicule mats shape macrobenthic diversity and act as a silicon trap. *Mar Ecol Prog Ser* 2013, **480:** 57-71.

52. Maldonado M, Carmona MC, Velásquez Z, Puig A, Cruzado A, López A*, et al.* Siliceous sponges as a silicon sink: An overlooked aspect of the benthopelagic coupling in the marine silicon cycle. *Limnol Oceanogr* 2005, **50**(3)**:** 799-809.

53. Chu JWF, Maldonado M, Yahel G, Leys SP. Glass sponge reefs as a silicon sink. *Mar Ecol Prog Ser* 2011, **441:** 1-14.

54. Maldonado M, Aguilar R, Bannister RJ, Bell JJ, Conway KW, Dayton PK*, et al.* Sponge grounds as key marine habitats: A synthetic review of types, structure, functional roles, and conservation concerns. In: Rossi S, Bramanti L, Gori A, Orejas C (eds). *Marine animal forests: The ecology of benthic biodiversity hotspots*. Springer International Publishing: Cham, 2017, pp 145-183.

55. Dayton PK. Interdecadal variation in an Antarctic sponge and its predator from oceanographic climate shifts. *Science* 1989, **245:** 1484-1486.

56. Maldonado M, Ribes M, Van Duyl FC. Nutrient fluxes through sponges: biology, budgets, and ecological implications. *Adv Mar Biol* 2012, **62:** 114-182.

57. Conway KW, Barrie JV, Austin WC, Luternauer JL. Holocene sponge bioherms on the western Canadian continental shelf. *Cont Shelf Res* 1991, **11**(8-10)**:** 771-790.

58. Jochum KP, Wang X, Vennemann TW, Sinha B, Müller WEG. Siliceous deep-sea sponge *Monorhaphis chuni*: A potential paleoclimate archive in ancient animals. *Chem Geol* 2012, **300-301:** 143-151.

59. Ragueneau O, Chauvaud L, Moriceau B, Leynaert A, Thouzeau G, Donval A*, et al.* Biodeposition by an invasive suspension feeder impacts the biogeochemical cycle of Si in a coastal ecosystem (Bay of Brest, France). *Biogeochemistry* 2005, **75**(1)**:** 19-41.

60. DeMaster DJ. The supply and accumulation of silica in the marine environment. *Geochim Cosmochim Acta* 1981, **45**(10)**:** 1715-1732.

61. Dutkiewicz A, Müller RD, O'Callaghan S, Jónasson H. Census of seafloor sediments in the world's ocean. *Geology* 2016, **43**(9)**:** 795-798.

62. Tréguer PJ. The Southern Ocean silica cycle. *C R Geoscience* 2014, **346**(11)**:** 279-286.

63. Bavestrello G, Bonito M, Sarà M. Silica content and spicular size variation during an annual cycle in *Chondrilla nucula* Schmidt (Porifera, Demospongiae) in the Ligurian Sea. *Scientia Marina* 1993, **57**(4)**:** 421-425.

64. Kamatani A, Oku O. Measuring biogenic silica in marine sediments. *Mar Chem* 2000, **68**(3)**:** 219-229.

65. Ehrlich H, Maldonado M, Parker AR, Kulchin YN, Schilling J, Köhler B*, et al.* Supercontinuum generation in naturally occurring glass sponges spicules. *Adv Opt Mater* 2016, **4**(10)**:** 1608-1613.

66. Gregoire G, Le Roy P, Ehrhold A, Jouet G, Garlan T. Control factors of Holocene sedimentary infilling in a semi-closed tidal estuarine-like system: the bay of Brest (France). *Marine Geology* 2017, **385**(Supplement C)**:** 84-100.

67. Miralles J, Radakovitch O, Aloisi JC. 210Pb sedimentation rates from the Northwestern Mediterranean margin. *Mar Geol* 2005, **216**(3)**:** 155-167.

68. Sumner EJ, Siti MI, McNeill LC, Talling PJ, Henstock TJ, Wynn RB*, et al.* Can turbidites be used to reconstruct a paleoearthquake record for the central Sumatran margin? *Geology* 2013, **41**(7)**:** 763-766.

69. Tenzer R, Gladkikh V. Assessment of density variations of marine sediments with ocean and sediment depths. *Sci World J* 2014, **2014:** 1-9.

70. Sandford F. Physical and chemical analysis of the siliceous skeletons in six sponges of two groups (demospongiae and hexactinellida). *Microscopy Research and Technique* 2003, **62**(4)**:** 336-355.

71. DeMaster DJ. The diagenesis of biogenic silica: Chemical transformations occurring in the water column, seabed, and crust. In: Mackenzie FT (ed). *Treatise on Geochemistry, Volume 7 : Sediments, diagenesis, and sedimentary rocks*, vol. 7. Elsevier, 2003, pp 97-98.

72. Hurd DC. Physical and chemical properties of siliceous skeletons. In: Aston SR (ed). *Silicon geochemistry and biochemistry*. Academic Press: London, 1983, pp 187-244.